TECHNICAL REVIEW

No.12 / October 2019

Technical Review

MAPNA TURBINE ENGINEERING & MANUFACTURING CO. (TUGA)

TUGA

MAPNA GROUP

Willpower to Empower Generations

Cover Page:

MGT-30 High Pressure Turbine Disk-Blade Assembly

Editorial

Dear Colleagues, Partners and Professionals,

A culture of dedication, innovation and intensive research and development has long been established and nurtured at MAPNA Turbine so as we spare no effort to provide proven solutions to any technical problem, and improve quality and reliability of our products and services. It is with great pleasure and immense honor that a brief account of a few recent achievements and technological breakthroughs is presented to you, our valued readers, in this edition of MAPNA Turbine Technical Review.

The first article is a thrilling success story in pinpointing and tackling the root causes of some reliability issues encountered with at times using early version of MGT-30 gas turbines. The DMAIC scheme as a proven data-driven improvement and problem-solving methodology has been employed to make sure that the problem is definitely solved and the related improvement processes are totally established and optimized over time.

The second article reviews design process, manufacturing and test of our gearbox developed for Air-Cooled Condenser (ACC) of MAPNA combined cycles. ACC gearboxes are important for steam turbine power generation cycles due to their direct impact on the condensing process. Mastering the design knowledge of such power plant accessories paves the way for further optimization and performance improvement of the equipment, and the whole plant.

With state-of-the-art MGT-75 gas turbine in development, with a combined cycle efficiency of around 59% in prospect, the third article outlines meticulous steps taken to design an entirely new set of Low Pressure End (LPE) steam turbine blades. Successful tests of the blades have made them ready to use for the Steam Turbine of the mentioned cycle, as well as future designs for further applications.

The fourth article features development of a robust protective coating with remarkably high abrasion and corrosion-resistant properties in dealing with water droplet erosion damages typically observed on gas turbine compressor blades operating with wet compression system. The AlCrN-PVD coating developed for this purpose has gone through extensive micro and macro structural analyses as well as hardness measurements to ensure high quality and durability of the developed protective coating.

Last but definitely not least, integration of the Chemiluminescence imaging technique as one of the simplest, most efficient and widely used optical methods for combustion diagnostics into the MAPNA Turbine combustion lab is laid out in the fifth article. In doing so, an experimental setup utilizing a premixed lab burner was developed and fine-tuned to carry out investigative measurements and to shed more light on combustion dynamics.

Please join us in relishing the detailed account of these subjects, in this issue of the Technical Review.

Respectfully,

Mohammad Owliya, PhD

Deputy General Director

MAPNA Turbine Company

(TUGA)

September 2019

Table of
Contents

03-12

1

DMAIC IN ACTION TO IMPROVE RELIABILITY OF MGT-30 MACHINES

13-20

2

GEAR UP TO THE NEXT LEVEL: ACC GBX DESIGN, MANUFACTURING & TEST

21-26

3

TF-37, NEW OUTSTANDING SET OF STEAM TURBINE LPE BLADES

27-32

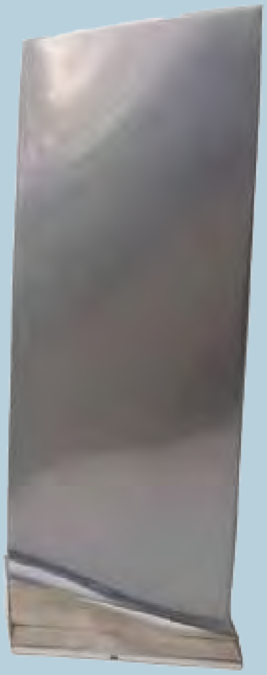

4

DEVELOPING ABRASION RESISTANT PVD COATING FOR TURBINE BLADES TO MITIGATE WATER DROPLET EROSION

33-38

5

EXPERIMENTAL INVESTIGATION OF FLAME CHEMILUMINESCENCE EMISSION

1

DMAIC in Action to Improve Reliability of MGT-30 Machines

Introduction

The three-spool gas turbine MGT-30 is a well-known machine with a large fleet in Iran deployed in strategic natural gas transmission lines as well as MAPNA stationary & mobile power plants.

Improving the reliability of this turbine has long been targeted at MAPNA Turbine through monitoring the units, studying the root causes of reliability issues and subsequently defining and implementing improvement plans. In this regard, reliability of High Pressure Turbine (HPT) blades in harsh conditions (including dusty and high temperature weather, with wet gas fuel and continuous peak load operational regime) was identified as an important area of improvement.

The DMAIC/DMADV methodology including 5 steps depicted in Fig. 1 was used to make sure that the improvement processes were truly applied and optimized over time.

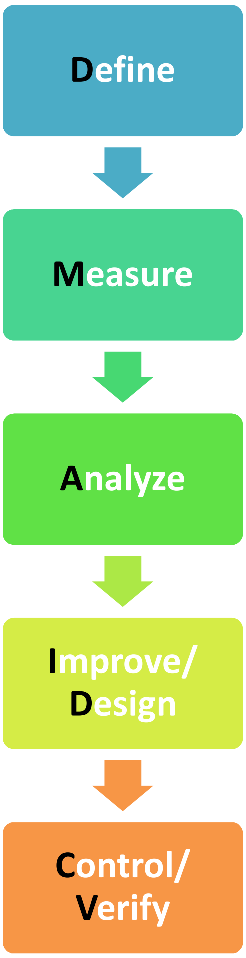

Fig. 1 – Schematic representation of DMAIC/DMADV methodology

Define

Based on the meetings held with stakeholders, the topic of the improvement project was defined as below:

"Increasing the reliability of the MGT-30 gas turbine in harsh conditions by resolving the HPT blade failure problem within 18 months."

And also below requirements were set to be considered:

- The manufacturing process of HPT blades should not be changed.
- Any Increase in the cost of HPT blades should be approved by internal stakeholders.
- The solutions should be gradually performed for all turbines with harsh operational conditions in the site or in the company workflow.

Measure & Analyze

Based on the Root Cause Analysis (RCA) process, the following parameters for two gas turbines with HPT blades failure and nearly eight gas turbines without any failure operating in harsh conditions were measured and analyzed.

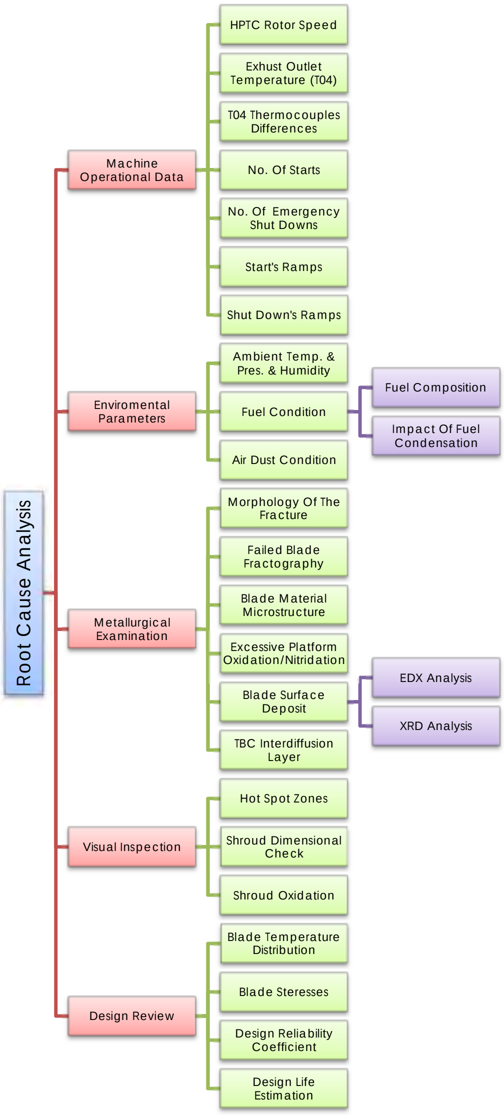

Fig. 2 – Schematic representation of the RCA performed on several MGT-30 gas turbines

Consequently, fact finding process showed that:

- The HPT blade(s) had failed due to creep deformation and cracking
- Excessive heat resulting in high metal temperature was the main reason for cracking of the blade(s)
- In comparison with the sound blades, the failed ones were exposed to higher temperatures by nearly 120 °C

Afterwards, to initialize the improvement, the problem was re-defined as below:

“Decreasing the temperature of blades by 120 °C in 18 months”.

Improvement

Improvement process involved brainstorming and prioritizing to get close to the possible solutions.

Topic	Narrower Topic	Solution(s)
Decreasing Blade Temprature »	Deposits »	I1: Enhancing the Air Intake Filtration Scheme from f7 to f9 I2: Inspecting (& Repairing) the Air Intake Sealing (If Needed)
	Cooling Air »	I3: Increasing Blade Secondary Cooling Air Flow Rate
	Coating »	I4: Increasing Thickness of the TBC Coating Layer I5: Utilizing New TBC Coating Layer
	Operational Conditions »	I6: Limiting Exhaust Outlet Temperature (T04)
	Blade Materials »	I7: Material Exchange
	Stress Levels Reduction »	I8: Increasing Blade Wall Thickness

Fig. 3 – Improvement process plan developed to tackle the problem of HPT blade failure in MGT-30 gas turbine

As the next step, the solutions were investigated. Studied parameters were included but not limited to: practicality, outcomes, probable risks, risk analysis and costs.

I1: Enhancing the Air Intake Filtration Scheme from f7 to f9

The deposits on the blade airfoil change the boundary layer and reduce the heat transfer, resulting in potentially hotter blades. Analyses show that the blade surface deposits largely contain the elements present in the surrounding soil (getting into the gas turbine through the air intake). Using a finer filter prevents dust from entering the machine and subsequently limits the deposit formation. What it takes, is ordering finer filters which makes it highly practical.

Associated Risks: None.

I2: Inspecting the Air Intake Sealing & Subsequent Repairs (As Required)

The blade surface deposits may be caused by insufficiency of the air intake sealing. The air intakes at sites with the HPT blade failure risk are needed to be inspected using the related checklists and repaired if defects are detected.

Associated Risks: None.

I3: Increasing Blade Secondary Cooling Air Flow Rate

Air flow rate through the HPT blades is increased by 15~20% through redesigning the cooling paths related to the HPT blades.

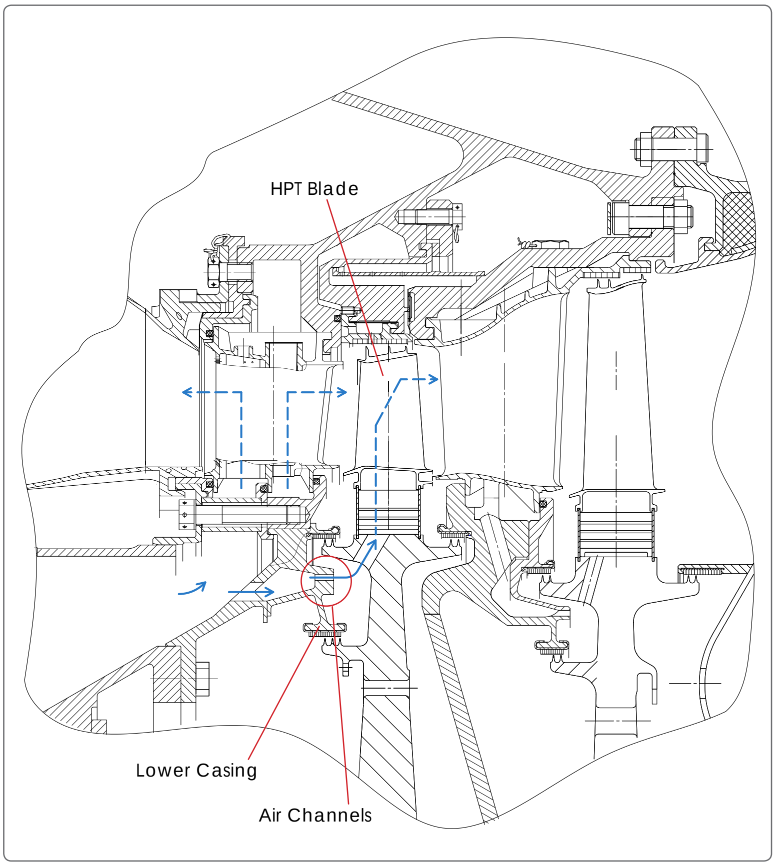

Fig. 4 – MGT-30 gas turbine HPT and blade air cooling paths

The amount of the cooling air flow rate going through the MGT-30 gas turbine HPT blades can be adjusted by the channels on the lower casing shown in Fig. 4. The cooling air flow rate increase through modified HPT blades requires the lower casing flow rate capacity increase by around 15 %. Consequently, the new design would require increased height of the air channels as well as additional ones.

The impact of such upgrades on the HPT blade temperature distribution is calculated and verified (by Design of Experience (DOE)) as shown in Fig. 5.

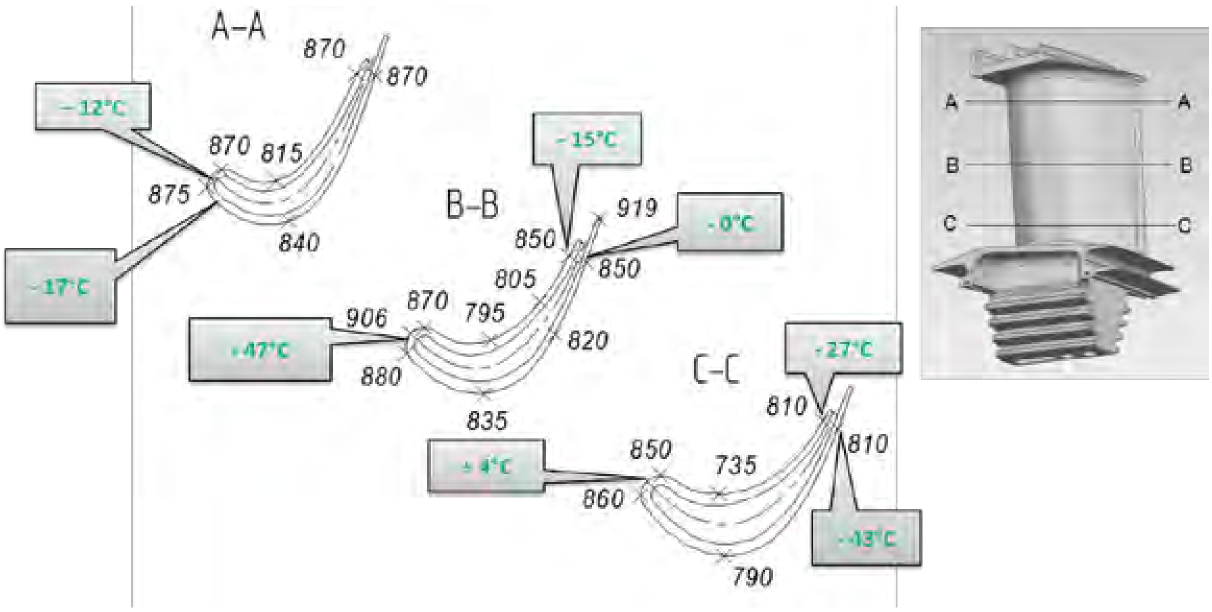

Fig. 5 – Schematic representation of the effects of increased cooling air flow rate on temperature distribution along the MGT-30 gas turbine 1st stage HPT blade

Associated Risks:

R1. Reducing Power Output and Efficiency

Efficiency drop caused by the increase in the secondary cooling air flow rate was calculated. It was less than 0.05 % and hence accepted. Likewise, the decrease in the output power was negligible.

R2. The Fault in the Calculation and Designed Test

Since the pilot test was not applicable to this solution, all calculations were re-performed by a third party using a different method.

I4: Increasing Thickness of the TBC Coating Layer

The thickness of the TBC coating of the failed blades was less than 70 microns and the coating method used was Low Vacuum Plasma Spraying (LVPS). Although it is possible to apply coatings as thick as 350 microns with this method, drawbacks such as decreasing the throat of blades and subsequent negative impacts on power, efficiency and machine run-up make this decision unreasonable. According to the investigations, 200-250 µm is the optimum range of coating thickness without any meaningful side effects. It's noteworthy that with this modification, surface temperature of each blade is expected to drop by nearly 40 °C.

Associated Risks:

R3. Negative Effects on Power, Efficiency and Machine Run-Up

According to the investigations, 200-250 µm is the optimum range of coating thickness without any conspicuous side effects. It was verified in a pilot test carried out in the factory test stand.

R4. Coating Detachment

In addition to diverse coating specifications, evaluation tests including microstructure investigation, bond strength measurements as well as quality of the coating applied on the upgraded HPT blades and their surface conditions were studied at two timeslots:

1. Short-term performance test (during factory tests): all manufactured turbines should be disassembled for inspection following completion of the factory operational tests. Inspections for 13 units- related to 1 year- showed that coating detachment was reported for 4 units. It was just related to 3 ~ 5 blades (among 86 blades) that had been replaced with the new blades. The new problem - to be solved through DMAIC/DMADV- was defined for coating spallation in these 4 units and eventually some preventive modifications were performed in the technological process of coating application.
2. During operation on site: There are periodic inspections on site at 2000, 4000, 8000 and 16000 Equivalent Operational Hours (EOH). Although there was not any report of significant coating detachment in any periodic inspections on sites, the pilot test for 4000 EOH was done for the first manufactured batch of upgraded HPT blades. Fig. 6 depicts MGT-30 gas turbine HPT blades with thicker coatings at 2000 EOH.

I5: Utilizing New TBC Coating Layer

In order to reach higher temperature gradient between the surface of the coating and underneath substrate, a new composite ceramic layer, was applied on HPT blades. Taking advantage of this coating, relevant thermal conductivity coefficient decreased by 68%. It stems from penetration of refractory oxides with higher melting temperature in the matrix of ceramic layer. As confirmed by the qualification tests, surface of the bond coat become rougher to acquire better TBC adhesion. The lower the temperature on the surface of the substrate, the better its resistance against high temperature oxidation.

Associated Risks:

The aforementioned risk, R4, is still there, but in lower levels. Fig. 6 depicts coating of the HPT blades using the new TBC coating layer after 2000 EOH.

Fig. 6 – A photo of the MGT-30 gas turbine HPT blades coated with a thicker layer of new TBC coating layer after 2000 EOH

I6: Limiting the Gas Generation Compartment Outlet Temperature (T04)

The compressor and turbine degradation drops the gas turbine performance which the operator would try to make up for by injecting more fuel (in some occasions) which would cause a higher metal temperature. To prevent this detrimental situation, the gas generation outlet temperature (T04) should be limited to maximum 750 °C. It's noteworthy that although the design temperature of T04 for gas fuel turbo generator is 740 °C, the units with failed HPT blades were operated with that temperature close to 770 °C.

Associated Risks: None.

I7: Material Exchange

Two different materials with purportedly superior creep properties were chosen to take the place of the existing material of the MGT-30 gas turbine HPT blades. A comparison between the creep strengths of these materials is presented in Fig. 7. As it is clear from Fig. 7, the 'S1' material withstands temperatures by nearly 20 °C higher than those of the other materials over the entire range of the stress magnitudes represented.

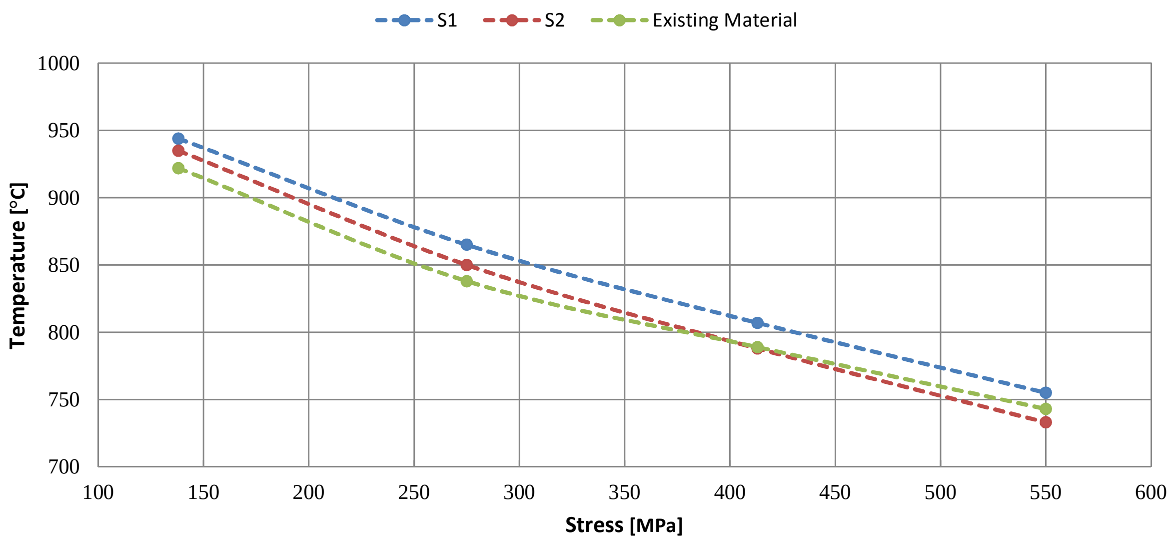

Fig. 7 – Creep strength vs. temperature for materials under investigation

Associated Risks:

R5. Less Corrosion Resistance

The ‘S1’ material has less corrosion resistance and in spite of the fact that it is not a good option for an offshore platform with severe corrosion conditions, it has been widely used in different gas turbine models presented by major OEMs.

R6. Higher Associated Costs

The manufacturing pilot test was carried out for just a single blade.

I8: Increasing Blade Wall Thickness

Our calculations show that increasing wall thickness in the failed section by 0.4 mm decreases maximum stress values by nearly 5% and subsequently improves blade creep life by nearly 3000 hours. According to the creep diagram, at the same stress and operational temperature values, 3000 hours increase in the creep life is equal to the temperature decrease of nearly 8 °C. The Von Mises stress values (MPa) around the crack-prone region of a typical HPT blade is shown in Fig. 8.

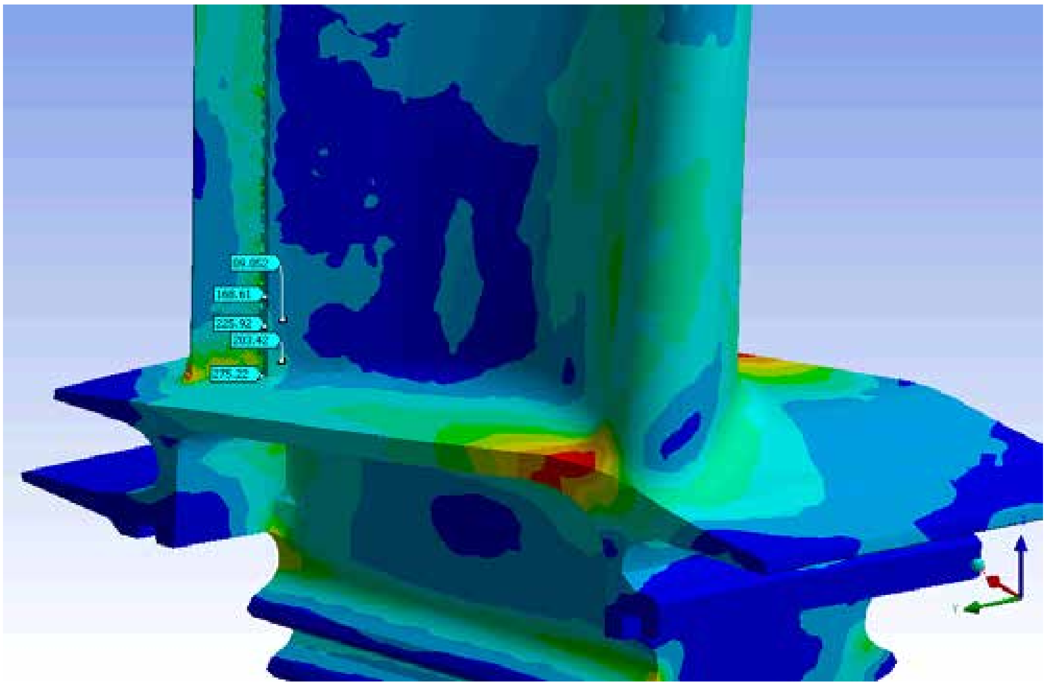

Fig. 8 – Von Mises stress values around the cracked region of MGT-30 gas turbine HPT blade

Associated Risks: Same as R3

A summary of all remedial actions taken along with the risks encountered and outcomes provided is presented in Table. 1.

Table 1 – Summary of the remedial actions taken to overcome MGT-30 gas turbine HPT blade failure

Item	Solution(s)	Risk(s)	Risk Level*1	Cost Ratio*2	Improvement/ Protection	Outcome(s)	Time	Control/ Verify	Pilot Test	Outcomes/Cost+Risk	Implementation Priority
I1	Change the air-intake filtration from f7 to f9	None	1	1	Pro.	-	short	No	No	-	**0**
I2	Inspect the air-intake sealing and repair (if needed.)	None	1	0	Pro.	-	short	No	No	-	**0**
I3	Increase the blade secondary cooling air flow rate.	R1&R2	2&2	3	Imp.	27°C	Long	Ver.	No	3.8	**5**
I4	Increase the thickness of TBC coating:	R3&R4	1&3	1	Imp.	40°C	Med.	Ctrl	Yes	8	**3**
I5	Utilizing new TBC coating layer	R3&R4	1&3	2	Imp.	60°C	Med.	Ctrl	Yes	10	**2**
I6	Limit the gas generation outlet temperature (T04)	None	1	0	Imp.	20°C	short	Ver.	No	10	**1**
I7	Change the material	R5&R6	6&4	3	Imp.	20°C	Long	Ver.	Yes	1.5	**6**
I8	Increase the blade wall thickness.	R3	1	0	Imp.	3000OH ≅8°C	Med.	Ver.	Yes	8	**4**

*1 According to the Standard Risk Matrix Classification, Risk Levels are classified into 4 levels on the basis of their score or calculation as shown below:

VERY HIGH (12,16)
HIGH (8,9)
MEDIUM (4,6)
LOW (1,2,3)

*2 Cost Ratio classifies the estimated cost into 5 levels as shown below:

High (4)
Medium (3)
Low (2)
Very Low (1)
No cost (0)

By implementation of the proposed solutions the temperature of the MGT-30 gas turbine HPT blade would be decreased by up to nearly 175 °C consistent with our objective of: “Decreasing the temperature of the blade by amount 120 °C within 18 months”.

Control

The Control section is all about putting processes and procedures in place to make sure the implementation of the new solution runs smoothly and can be tracked and optimized over time. At the first step the results of the cost-benefit ratio and risk analyses paved the way to prioritize the implementation of the solutions as presented in Table. 1

The next step was to make sure that the new solutions were effectively integrated into the company workflow in practice. To achieve this, the following steps were followed:

- Documents required to perform solutions were prepared and issued officially
- The units with harsh condition (with risk of HPT blade failure) were specifically identified
- The materials needed to perform solutions were ordered and supplied
- Documents, bill of materials, technical processes and qualification procedures needed for implementation of the solutions were defined and uploaded to the MAPNA Turbine's Enterprise Resource Planning (ERP) software to systematically ascertain that the modifications are incorporated into the company workflow

Finally, the modifications have been being monitored to make sure the problems are resolved.

A roadmap representing the outcomes associated with each of the solutions provided (in terms of temperature decrease) and the amount of time required for application of each by the order of their priorities is represented in Fig. 9.

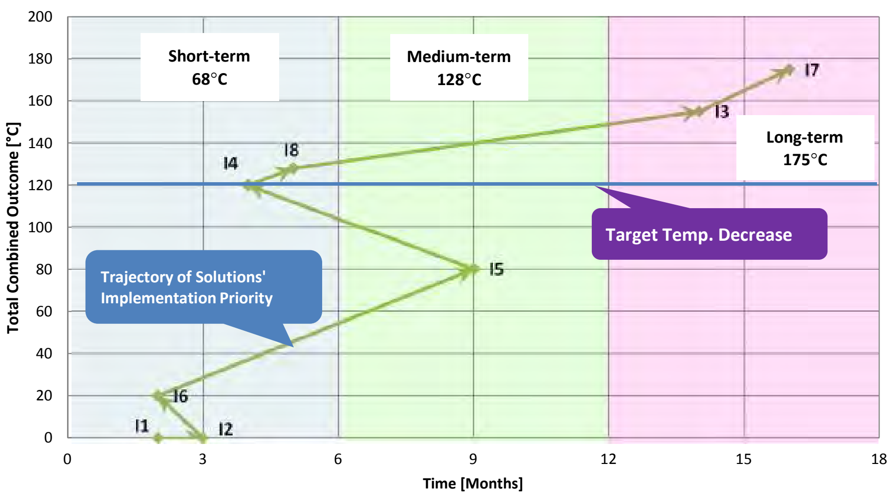

Implementation Priority	Solution	Outcome [°C]	Net Combined Outcome [°C]
0	I1	Pro.	0
0	I2	Pro.	0
1	I6	20	20
2	I5	60	80
3	I4	40	120
4	I8	80	128
5	I3	27	155
6	I7	20	175

Fig. 9 – Outcomes associated with each of the solutions provided to overcome MGT-30 gas turbine HPT blade failure over time

Concluding Remarks

Improving the reliability of turbomachinery products is among MAPNA Turbine's long-term goals. Notwithstanding all technical issues, taking advantage of innovative and proven problem-solving methodologies is also essential to reach the desired outcomes. It is in this perspective that the DMAIC/DMADV methodology has been used for increasing the reliability of MGT-30 gas turbine's HPT blades. It serves as a roadmap to identify best practices to reach perfect results and processes while minimizing the errors and reducing time and cost of improvement projects.

Prior to the implementation of this improvement project, HPT blade failure had occurred in two MGT-30 gas turbines at almost 8000 hours EOH. Following the project and by implementation of some of the solutions provided on a fleet of 37 MGT-30 gas turbine units there has not been any HPT blade failure reported so far, with the maximum EOH reaching to almost 18000 hours.

2

Gear Up to the Next Level: ACC GBX Design, Manufacturing and Test

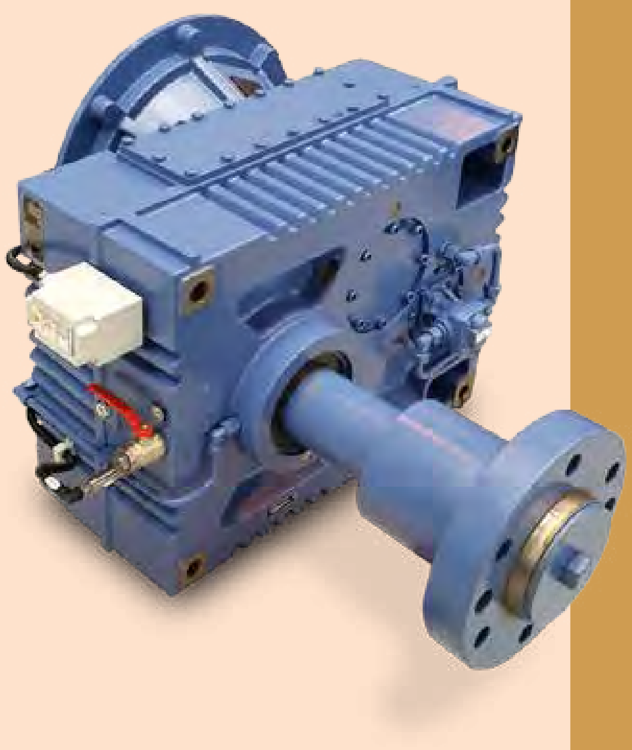

Introduction

As a major company in the field of power generation, MAPNA Turbine has always sought to extend the knowledge of designing and manufacturing power plant accessories and auxiliary equipment. Air-cooled condensers (ACC) are among important modules associated with steam turbines. ACCs have substantial impact on the overall efficiency of steam turbine power generation cycles due to their direct impact on the condensing process.

Power plant gearboxes are generally designed and manufactured with a high level of safety and accuracy. High accuracy grade and precise profile modifications for gears, special bearings, uniform casings, precise machining and strict assembling processes are among significant measures taken into account in manufacturing these items. Moreover, the reliable and continuous working of these units is essential given the special conditions and important job of these parts. MAPNA Turbine wealth of experience in design and manufacturing of special and precise instruments for a variety of applications means that by extending their gear design knowledge and thus opening a new field of activity, it would be possible to not only optimize the design and manufacturing process of these parts, but also significantly reduce the lead time and cost. To bring significance of the ACC gearboxes into perspective, it is to be mentioned that these pieces are generally designed for some twenty years of continuous service.

ACC System Overview

The low pressure steam flowing out of the steam turbine is condensed within the ACC in contact with the air flow. This system is a direct dry cooling device. In the ACC system, the output steam is directed through "A" type condensers through which the air flows across as well. The flowing air reduces the steam temperature and hence condensation takes place. An outline the ACC system gear box assembly is shown in Fig. 1. Several photos of the ACC system representing different parts including the structure, A-type condensers as well as the cooling fan are represented in Fig. 2.

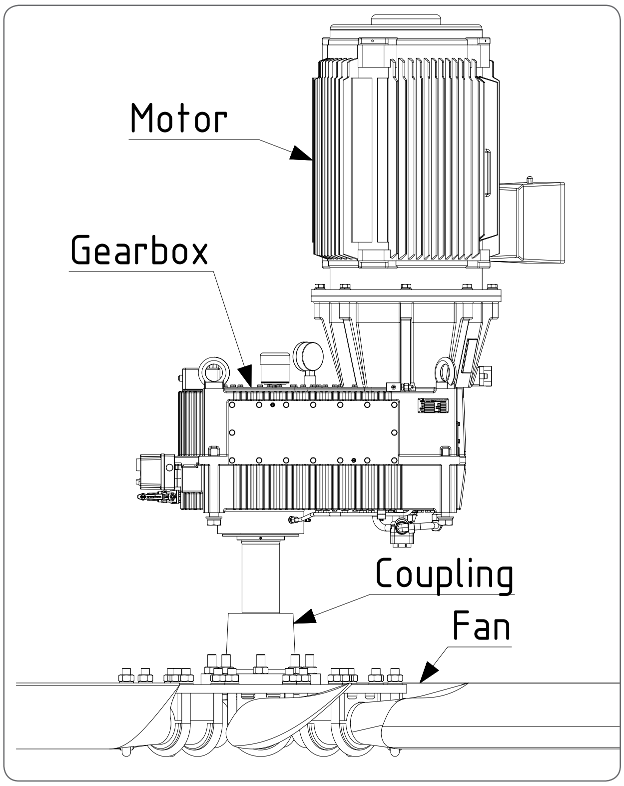

Fig. 1 – Outline of the ACC system gear box assembly

Fig. 2 – Photos of the ACC system representing, A-type condensers (left), the structure (middle) and the cooling fan (right)

The ACC system mainly consists of three sections including steam and condensate collection piping systems as well as the air flow generator. The main components of the air flow generator are shown schematically in Fig. 3.

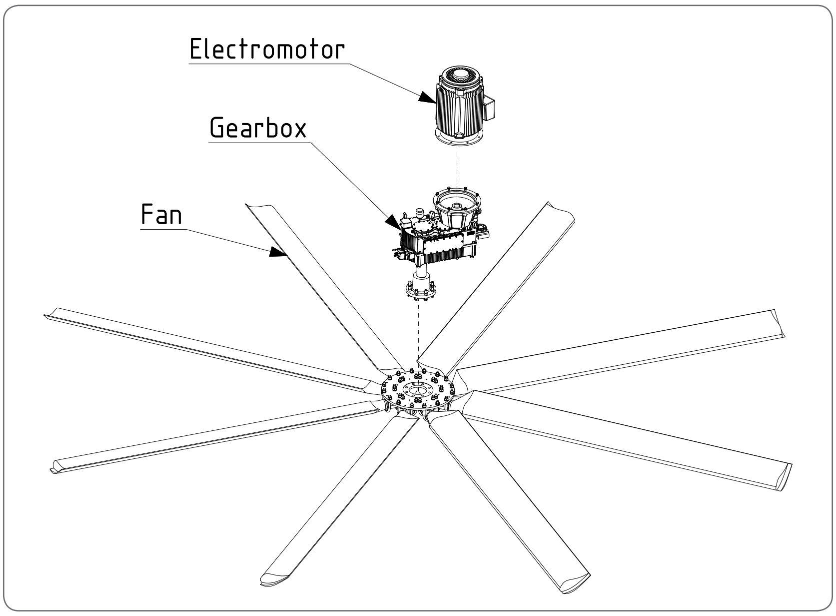

Fig. 3 – Main components of the air flow generator

In the air flow system, the large low-speed fan accounts for the air displacement. The diameter of the fan is about 9 meters and the thrust load is applied to the output shaft directly. The required power is generated by an electromotor and a reduction ratio gearbox. As the ultimate state of the condensing process has a direct impact on the overall efficiency of the steam turbine, the efficient and uniform performance of the fan is of particular importance.

ACC Gearbox Overview

The ACC gearbox is a two-stage gearbox with a reduction ratio typically in the range of 12-16 and mechanical efficiency of 98%. The gears are helical type with the accuracy grade of AGMA 6. The bearings are of roller type with combined splash and force-feed lubrication system. The lifetime of the gearbox is also around 180000 hours. A 3D representation of the ACC system gearbox is depicted in Fig. 4.

Fig. 4 – 3D representation of the ACC system gearbox

Some of the significant characteristics of the gearbox could be listed as follows:

Uniform casing, combined lubrication system, special sealing of the output shaft regarding the vertical orientation of the shafts as well as supporting all generated loads applied to the gearbox by the motor and the fan, are among some of the major characteristics of the ACC gearbox.

Design Procedure

The design process encompasses a few of steps taken ranging from the clarification process of the input data to the finalization of the gearbox outline and all accessories. A brief account of the main design procedures followed is presented below:

- **System Engineering Design Process**

The "System Engineering Design Method" is based on the concept of design purpose. In this method, all different levels of a product are needed to be categorized and identified as header levels, sub-levels and individual parts. The overall purpose of each part has to be specified and regarding its application, the criticality of each part could be established. This process ensures a high quality, reliable and convenient design process.

This process begins with completing a few information forms, and the overall result can be established in a multi-level diagram. A typical multi-level diagram is presented in Fig. 5.

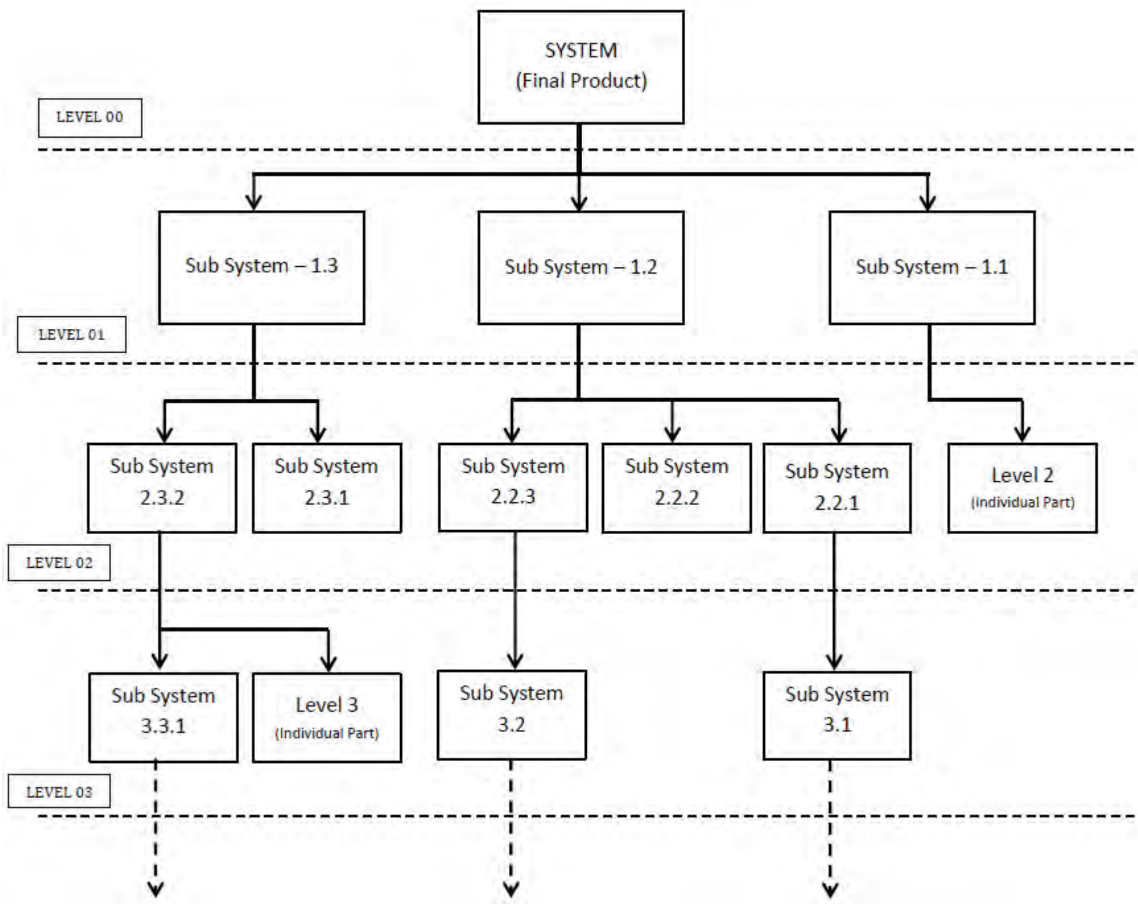

Fig. 5 – A typical multi-level diagram developed in the process of system engineering design method

- **Preliminary Design**

The first step to design a gear is to fully understand the entire design as a product. Therefore, it is crucial to consider all requirements of the product in line with the specific customer's order. The main steps in the early design process is using the input/output data and then sizing the gearbox accordingly.

The input data is usually provided by the customer. It includes all the necessary information such as power (input and output), service factor, reduction ratio, required lifetime and other parameters. This information has to be processed precisely in order to initiate the design process.

- **Gearbox Sizing**

Gearbox Sizing comprises any process which involves element selection or shape estimation. To be more specific, the gear size and the length of casing estimation is specified during this process.

The ACC Gearbox is a two-stage gearbox. Therefore, regarding the requested gear ratio, an appropriate gear sizing, ratio and power distribution between the two stages is to be implemented. This process was performed using KISSsys gear sizing section. A table of the best possible choices is proposed by the software and regarding the allowable center distance (referring to the available space around the gearbox) and the achieved safety levels, one of the gear pairs is selected.

Another important aspect is specifying gear contact angles. This parameter directly affects the casing size as it is clearly shown in Fig. 6. In order to choose the best possible contact angle, the longitudinal and lateral available spaces have to be taken into account.

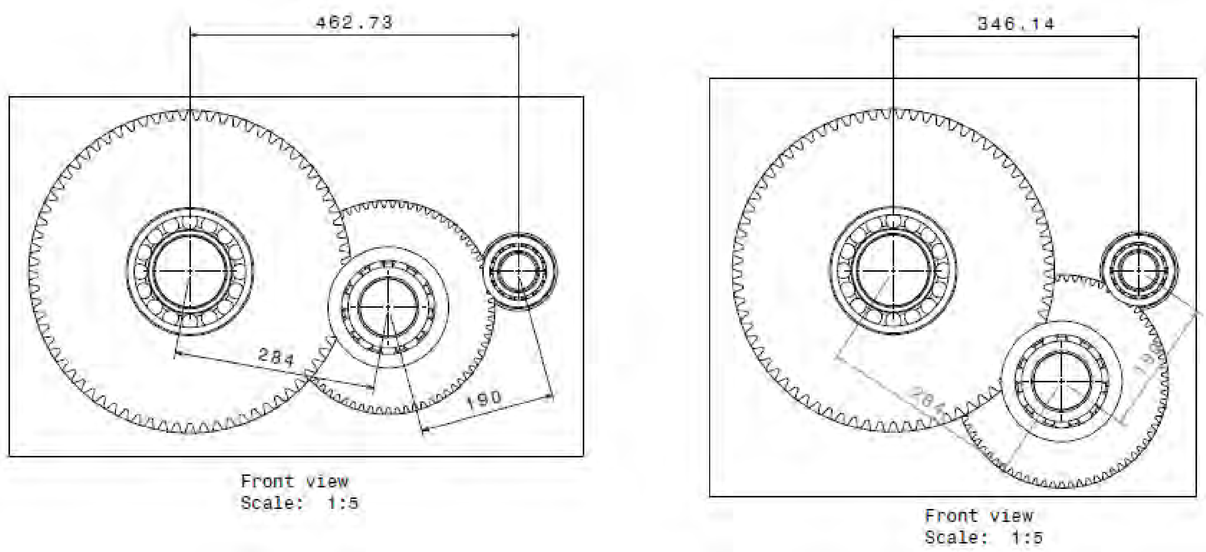

Fig. 6 – Gear outline representing impact of the contact angle on the overall size of the gear casing

- **Gearbox Elements Design**

The first step in designing gearbox elements was to generate a complete gearbox model in KISSsys using the input data. In this process, all the elements are designed and developed in accordance with the preliminary design.

Stepping through the design tree, all the components are calculated and designed with all necessary details. It is worth mentioning that the torsional frequencies of the internal components are calculated and taken into account so as to avoid occurrence of any resonance within the gearbox service speeds.

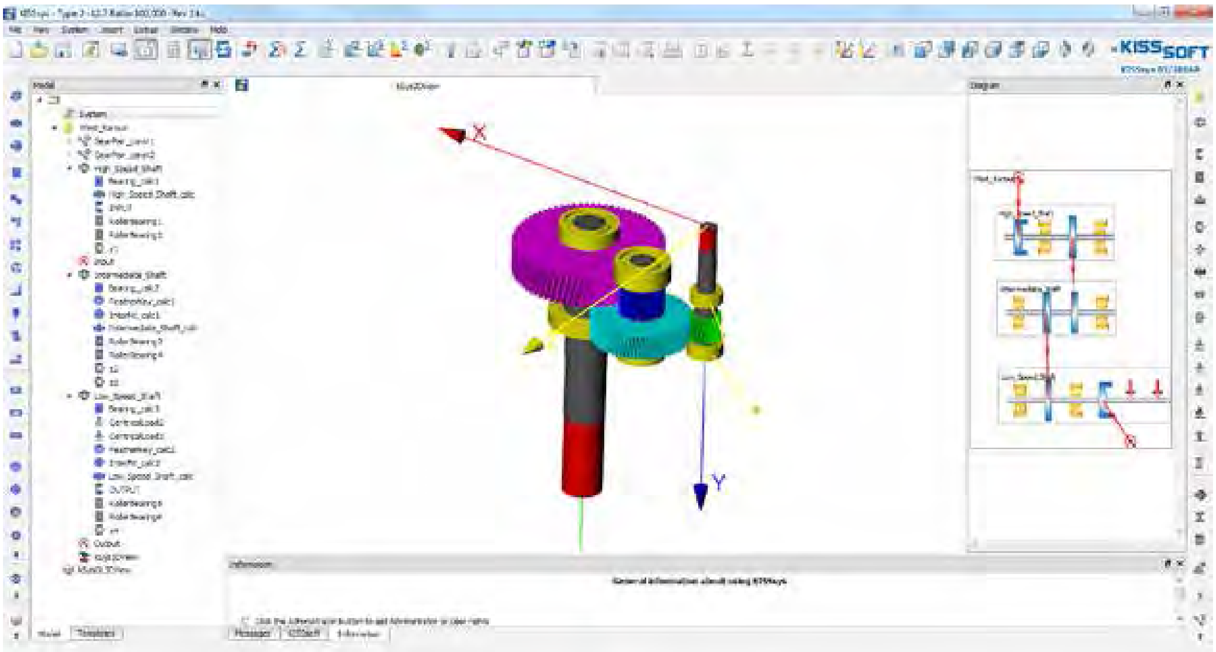

Fig. 7 – Gearbox elements design in progress using KISSsys software

- Gears

Gear design consists of two major steps: gear geometry design, and gear modification calculations. In terms of gear geometry, gear thickness, profile shift coefficient, accuracy, tool profile parameters, and calculation method regarding the tolerance standards must be specified and the result is gear safety level. As far as gear modification is concerned, tip relief, crowning, and helix angle modifications are applied to the original profile in order to reach a uniform contact. Typical tooth stress contours and corresponding transmission error diagram for the designed gear are presented in Fig. 8.

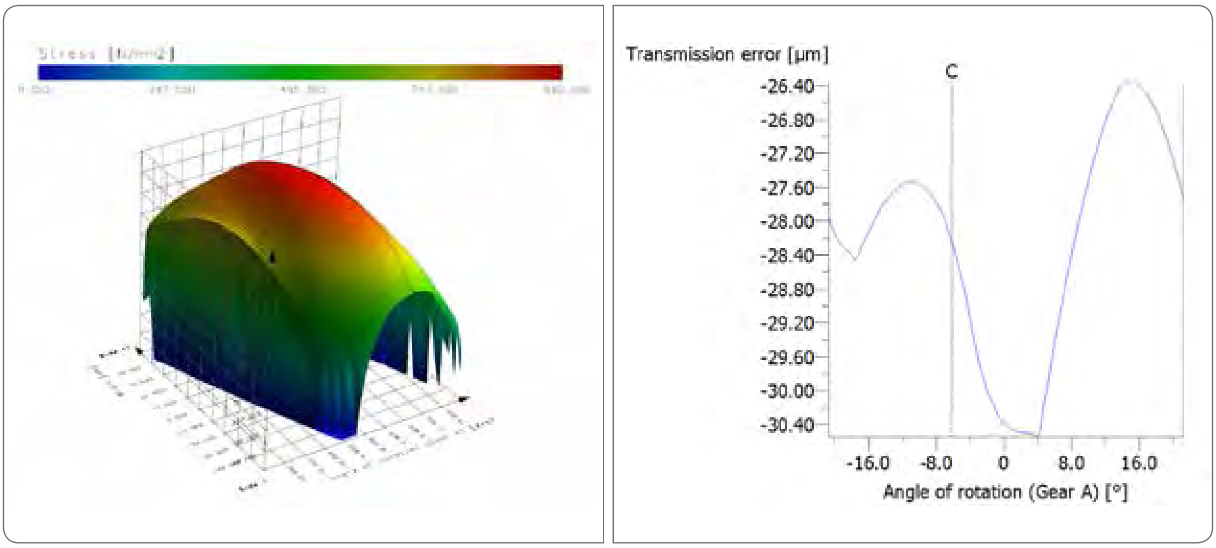

Fig. 8 – Typical tooth stress contours (left) and a transmission error diagram (right) of the designed gear

The standards used for the design of the gear were AGMA 2015 in terms of accuracy, DIN 3967 cd25 in terms of tolerances and AGMA 2101 D04 for the calculation method.

- Shafts and Bearings

Shafts and bearings design and calculation were performed with regard to the gear contact angles. The deformation of all elements was taken into account and all bending and torsional stresses and shear forces were also considered and included in calculations. Typical shaft stress and bearing force diagrams are presented in Fig. 9 for the designed gear assembly.

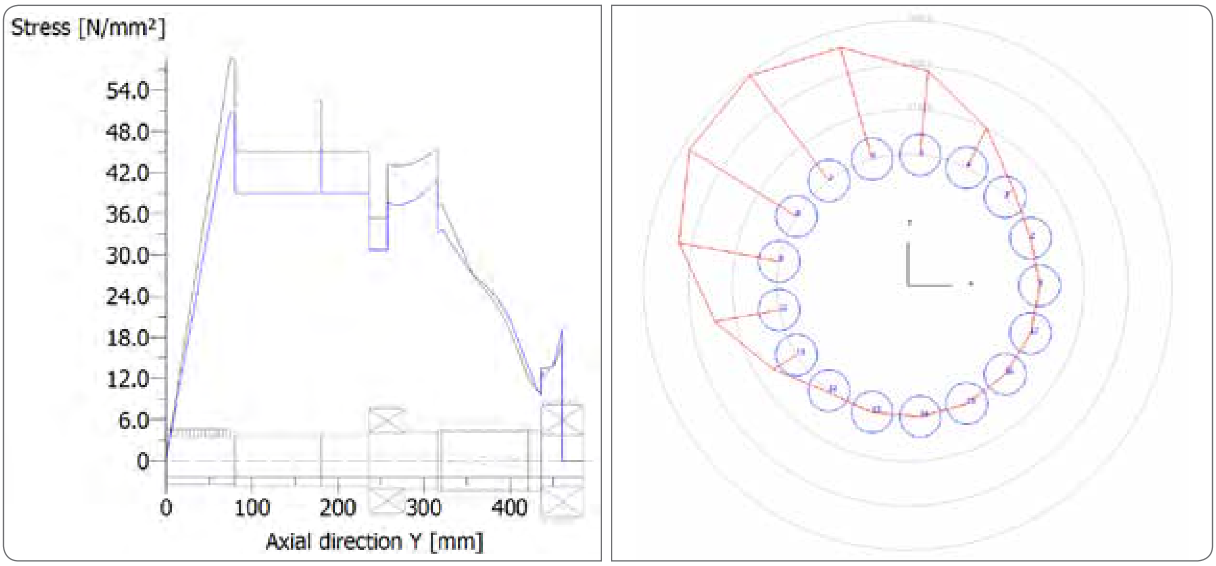

Fig. 9 – Typical shaft stress (left) and bearing forces (right) diagrams of the designed gear assembly

The gearbox shafts were designed according to DIN 743. The selection of the bearings was carried out in accordance with the guidelines of the SKF standards and service lifetime of the bearings was also reflected on, in accordance with the guidelines of the ISO 16281 international standard.

- Casing

The main character of the ACC gearbox casing was a uniform design. The casing material was chosen to be EN-GJS-500. The uniform design helps to achieve a precise casing following the machining process and regarding no-slip surfaces, the unwanted vibrations would be damped and kept at a minimum level. In order to design a casing with significant strength characteristics, static and vibrational analyses were implemented by means of Finite Element Method (FEM). In the static analyses, forces and torques due to electromotor, fan, and gears on the casing were evaluated. Frequency analyses near critical natural modes regarding unbalanced forces applied by the electromotor were carried out and dealt with through the vibrational analyses.

- **Gearbox Manufacturing Process**

The ACC gearbox was manufactured using state-of-the-art precision manufacturing tools, devices and equipment MAPNA Turbine is taking advantage of, following strict quality control procedures.

- **Approval Tests**

The main idea of a testing procedure is to verify the expected service of the equipment under real operating conditions. As it is not possible to test gearbox performance in the long run, some crucial parameters are controlled and recorded during the tests. These parameters could be different from a gearbox to another regarding the working condition, but generally, vibration on different directions on bearing housing, oil and bearing temperatures, oil pressure, and noise levels are of particular concern. The allowable limits are also specified regarding the real operating conditions. For the current ACC gearbox the acceptable extremes are as follows: 2.5 mm/s for vibration, 85 db for noise level, and maximum temperature of 90 °C for oil bath.

For the first manufactured gearbox, it is important to check the gear mesh contact pattern. This would reveal the correct form of designed gear modification.

Concluding Remarks

The ACC gearbox design and manufacturing process is a multi-level procedure. The first step is a system detail design to get a guideline for all levels of the product. In addition, it is important to create a preliminary design sketch covering all necessary characteristics regarding the input/output data. The next step is detailed design process and finally, a performance test in order to finish off the entire process.

Given the crucial role of the ACC gearbox in the cooling system and the impact of the cooling quality on the overall efficiency of a steam turbine, the design and manufacturing processes have to be kept at a high precision level getting continuous feedback from the stricter test/operation results in the near future.

3

TF-37, New Outstanding Set of Steam Turbine LPE Blades

Introduction

In order to increase the efficiency of MGT-75 – Latest F-Class gas turbine developed by MAPNA Turbine - in a combined cycle power plant block, it was decided to introduce a new steam turbine to win a combined cycle efficiency of about 58.9% at standard ISO conditions. The configuration to start with was assumed to be 1x1 meaning each single gas turbine train supplies hot gas to one steam turbine via a heat recovery steam generator (HRSG). This arrangement was chosen to address clients with relatively low budget, still looking for higher efficiency levels.

The steam turbine produces about 103 MW in the mentioned circumstances, with three-level-pressure boiler, reheat cycle and a quite high vacuum. However, in typical sites around Iran with an approximate condenser pressure of about 0.12 bara, the LPE (Low Pressure End) segment of the steam turbine must be selected or designed so that the exhaust loss is its absolute minimum.

Once the thermodynamic calculations of the cycle Heat Balance Diagram (HBD) were carried out, an annulus area of 3.7 m^2 was deemed to be fit for the job in such an application. However, this was not among MAPNA Turbine's LPE blade repository, nor even close to a ready-to-go set of blades and as a result, decision was made to design a brand new set of LPE blades from scratch, that involves the ending three stages of the steam turbine's LP section.

It is to be noted that, even major OEMs try to rely on their already proven sets of blades, as this critical stage of steam turbine design takes quite a bit of effort to finalize. On top of passing the aerodynamic criteria successfully the blading needs to be within mechanical and vibration constraints. As a matter of fact, the final product has to be operationally safe given all key aspects. It is interesting to know that the centrifugal forces applied on the root of each last stage blade of this set would be roughly 200 tons, which is more than twice as high as the whole body of the steam turbine. Moreover, since these blades are rather long, they are very likely to suffer fractures due to intense vibrations which give rise to High Cycle Fatigue (HCF). In brief, designing a new set of free-standing LPE blades was determined as the primary target of this project.

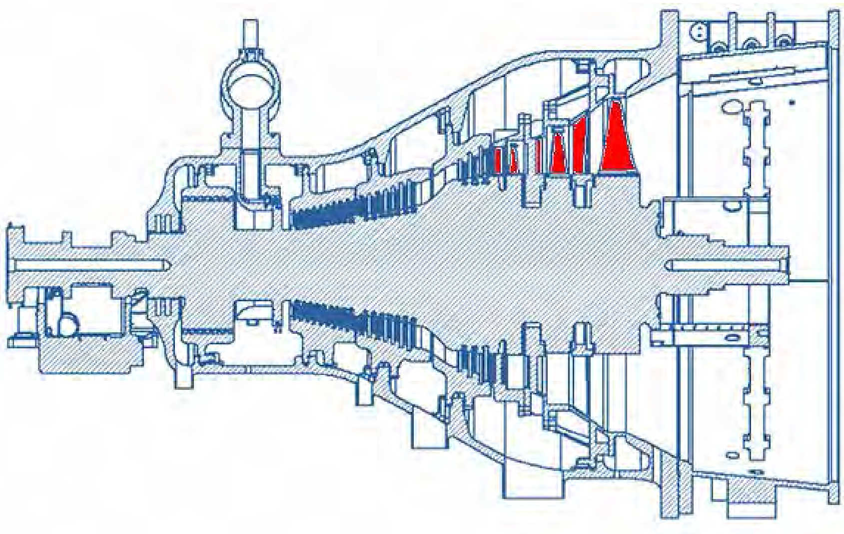

Fig. 1 – Schematic representation of a typical steam turbine cross-section

Aerodynamic Design

We had a two-pressure steam turbine with an exhaust annulus area of 5 m^2. However, it was not feasible to make use of its LPE blades as they were too large for a three-pressure 103 MW steam turbine we intended to design, in spite of the fact that the output powers of both machines were approximately the same.

Needless to say that we were not able to simply scale the blade down to create our required set as the rotational speed was kept the same. In a case where all lengths are downscaled and the rotor nominal speed is reversely proportioned, nothing needs to be changed and the smaller blades are proven to fulfill both aerodynamic and mechanical requirements.

It is not a good practice to consider reduction gear for power generation applications, as this would come off as a serious disadvantage to potential clients, not to mention higher costs, longer turbine footprint, additional noise, etc. Therefore the aim was to customize the original blades into a smaller size with optimum performance. This means that the airfoil metal angles had to be tailor-made specially for the new steam flow.

The original airfoil was first scaled down and then a consistency analysis was performed to find out the fewest possible cross sections for optimization procedure, so that the CFD calculations would be carried out without any major difficulties.

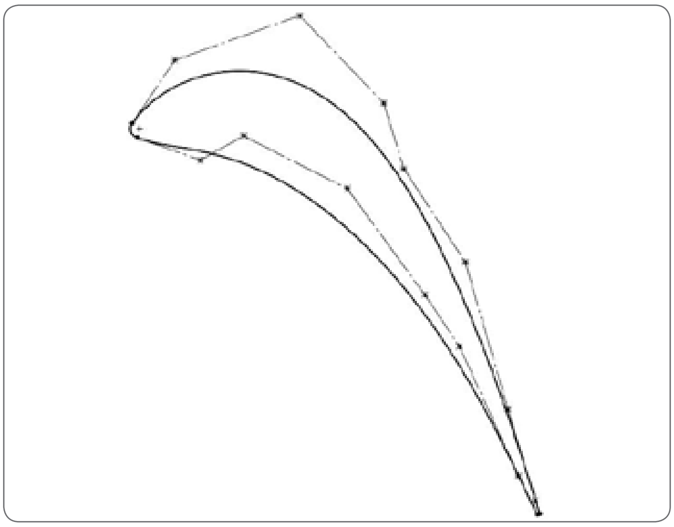

Fig. 2 – Representation of Bezier control points put on a typical airfoil cross section

Consequently, five cross sections were selected for the job, the first of which was located at the blade hub, and the last, at the tip. Another consistency analysis was also carried out to determine the fewest required control points (Fig. 2) to customize the section Camber line and thickness for the new conditions. Later, we came down to eight points for each (eight points for thickness and another group of eight for each section side, i.e. pressure and suction sides), as it is clearly observed in the diagrams presented in Fig. 3. The genetic algorithm was deployed as the optimization method. The location of the Bezier control points or the thickness values were the input parameters for the optimization study.

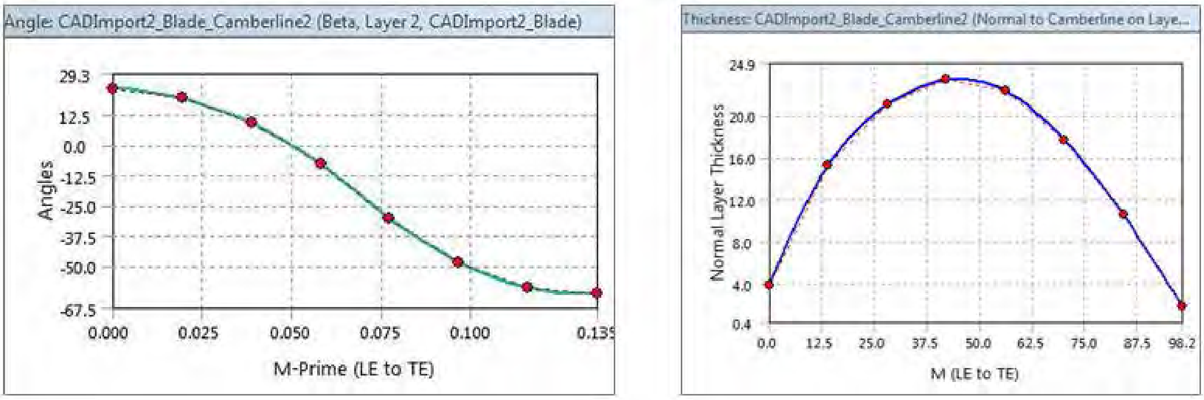

Fig. 3 – Metal angle and thickness values from the Leading Edge (LE) to the Trailing Edge (TE) of the blade

Due to the fact that this was our first experience in designing a brand new set of LPE blades, the optimization procedure was repeated for more than 30 times with different assumptions and circumstances.

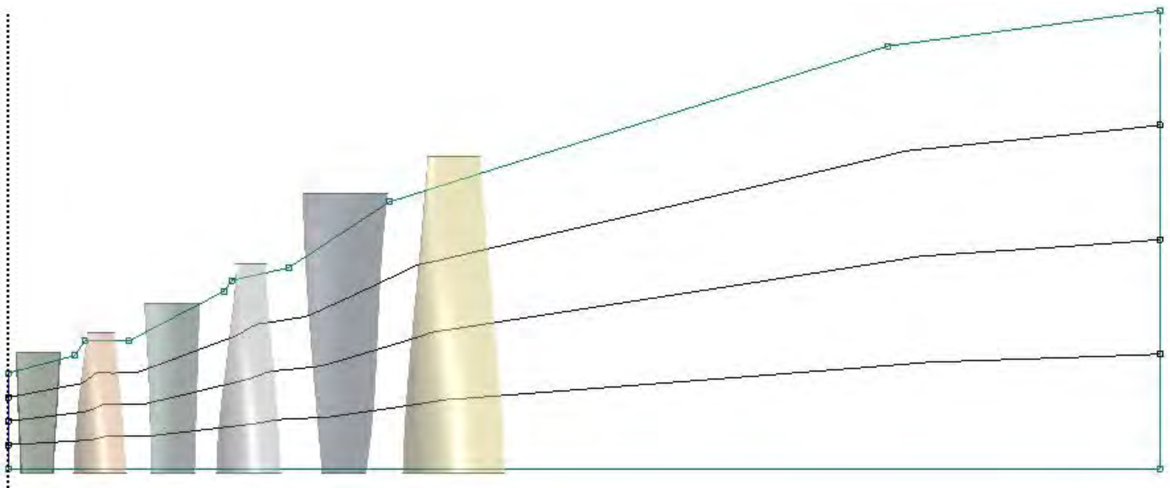

Fig. 4 – Steam flow path following completion of the optimization procedure

At each try, the values of the input parameters were changed within a pre-defined limit and then CFD calculations were implemented to investigate the performance status. Finally, the best case was selected as the output.

Mechanical Design

The mechanical aspect of the new blades including stress endurance limit and natural frequencies are not any less important than the performance of the blades. Parts of re-designing processes of the airfoil were due to the fact that the natural frequencies, either the first mode or the second, were too close to the nominal speed harmonics of the rotor. Those frequencies must be well far from the harmonics; otherwise the blades may vibrate intensely at the nominal speed and hence blade fracture may follow which would cost a fortune.

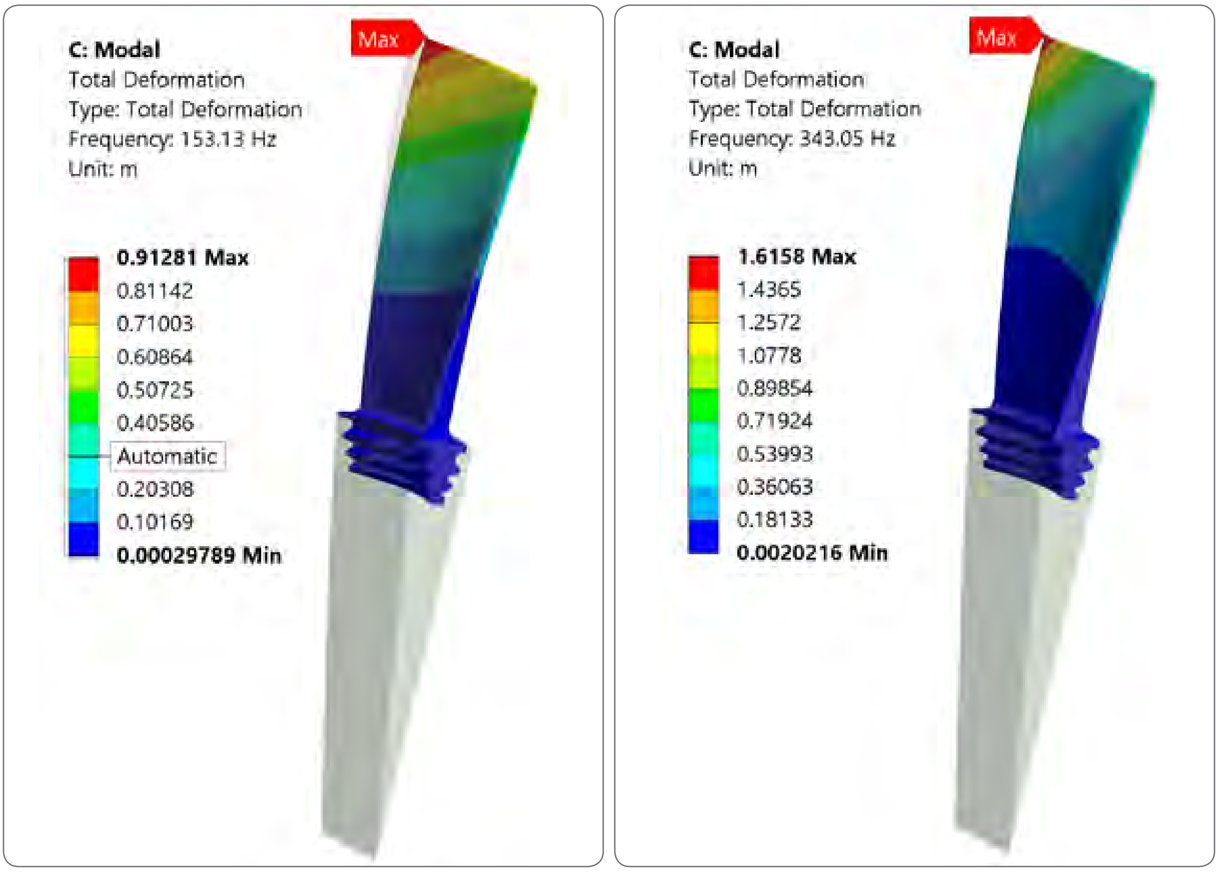

Fig. 5 – Natural frequency analyses carried out on the last stage blade

The results of the natural frequency analyses performed on the last stage blade in the static state are presented in Fig. 5, with 153.13 Hz and 343.05 Hz as the natural frequencies of the first and second modes, respectively. Moreover, it had to be checked to make sure that the vibration of the blade cascade or the entire blade row would not cause any mechanical problem. This was achieved through in-depth analyses carried out. In doing so, nodal diameters of the blade row, taking into account the number of corresponding stationary nozzles upstream and downstream of the blade, were assumed as an input to the HCF analysis performed. According to the results and as presented in Fig. 6, there was no serious concern in this regard at any given operating conditions.

The term “LEO” in Fig. 6 stands for ‘Low Engine Order’ excitation which deals with rotor harmonics up to the eighth order, and the term “NPF” stands for ‘Nozzle Passing Frequencies’ which implies the frequencies excited by the upstream and downstream stationary blades, i.e., the number of those nozzles multiplied by the rotational speed of the rotor. In fact, this is an excitation made by the flow wakes created at the leading edges of the downstream nozzles as well as those at the trailing edges of the upstream ones.

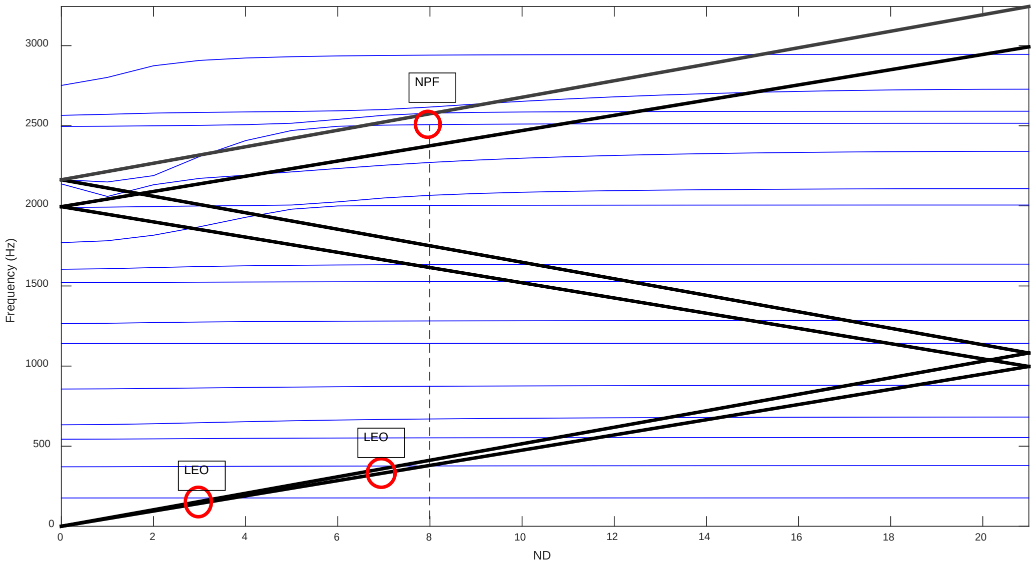

Fig. 6 – SAFE diagram of the LR-0 blade

The designed blades were also checked for the mechanical stresses mainly induced by the centrifugal forces applied on the roots, as shown in Fig. 7. They turned out to be strong enough to withstand the operating conditions. In order to check this out, the location of the airfoil center of gravity was tuned relative to that of the root in order to have equally stressed flanks at the pressure and suction sides.

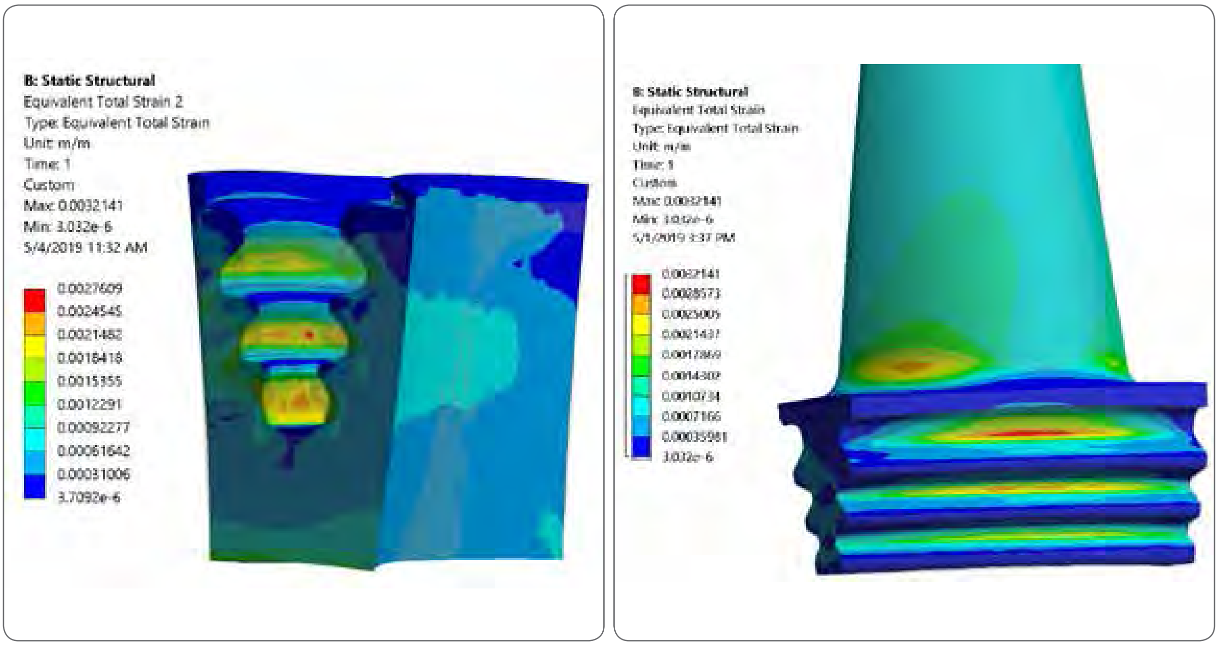

Fig. 7 – Strain contours at the LR-0 blade on the root and rotor groove

Concluding Remarks

A new set of LPE blades providing an annulus area of about 3.7 m^2 was designed and tested, that can be used both in MST-40C steam turbine and other machines for power generation applications. This is a major breakthrough in the design and development of new steam turbines that will be followed by the design of upstream sections of the steam path. This set of LPE blades can serve in steam turbines from approximately 50 MW to 110 MW of power, although other parameters such as condenser pressure, mass flow rate, and site conditions are also important when it comes to the selection of an appropriate set of LPE blades.

4

Developing Abrasion Resistant PVD Coating for Turbine Blades to Mitigate Water Droplet Erosion

Introduction

Abrasion and corrosion are the most prevalent damage mechanisms activated by collision of high speed droplets of sprayed water [1]. Upgrading the mechanical properties of the materials as well as applying protective surface coatings could be taken advantage of to prevent such damages. Improving the properties of the base material would generally result in huge costs and is hence not considered as an economically viable solution. Furthermore, recent studies show that 80% of the total costs of the protection of metals are related to coating application [2]. Abrasion resistant coatings are of surface coating systems which not only provide strong adhesion to the substrate but also show remarkable corrosion resistant properties in highly humid media. The emerging technology of developing such coatings is still under investigation and researchers are exploring field survey-based results to come up with more efficient approaches and schemes. Physical Vapor Deposition (PVD) method provides a promising ground for applying these abrasive coatings by formation of a dense adhesive film at a low deposition temperature. In addition to its erosion properties since the commercialization of TiN-PVD coatings in the early 1980s, proven corrosion protection capability of PVD coatings based on chromium and aluminum nitrates has been extensively reported in the literature [2].

Following the implementation of wet compression system in MGT-70 heavy-duty gas turbines, MAPNA Turbine has also launched a research project to develop abrasion resistant coatings for affected parts or materials, adversely impacted when using wet compression system. So, a thorough investigation of protective coating systems has been conducted and following the selection of an appropriate system (AlCrN) and application method (PVD), preliminary and supplementary examinations have been carried out in collaboration with the Iranian Nanotechnology Initiative Council and the SEVIN Plasma surface engineering company.

The results demonstrated efficient and robust performance of the coating system applied and boded well for the advantageous application in tandem with the advanced wet compression system deployed in the fleet of MGT-70 heavy-duty gas turbines.

Base Material and Coating Selected

- **Base Material**

The investigations show that the first stage of the compressor blades are largely affected by wet compression system and explicitly suffer from both abrasion and corrosion damage mechanisms. These blades are made of X4CrNiMo16-5-1; Martensitic Stainless Steel; a highly recommended appropriate material for compressor rotary blades due to its distinctive mechanical properties.

- **Coating Application Method**

Since the aim of the present research was developing a multifunctional (abrasion and corrosion resistant) coating with a superior surface profile, PVD technique was chosen as the coating application method. As reported in the literature, PVD coatings based on chromium and aluminum nitrates represent robust erosion and corrosion-resistant properties [3]. It is also established that in order to optimize coating layer properties, multi-layered microstructure blocking open porosities (grown in columnar structure using PVD method) and diffusion channels shall be formed [4]. So, the coating was applied on prepared surfaces using a pre-programmed chamber for formation of multi-layered microstructures to be accomplished. It is to be mentioned that, the minimum vacuum level of chamber for maintaining the quality and consistency of the coating applied was kept at 10-5 mbar during the procedure. Another issue with coating application procedure is to prevent coating deposition on unintended surfaces e.g., blade root leading to loss of energy and time and higher cost. So, a special fixture was also designed and manufactured to make it possible to properly place the blade inside the chamber. Consequently, the blade was taken out of the chamber after sufficient amount of time upon completion of the coating application procedure.

The coating application procedure was carried out in collaboration with the Iranian Nanotechnology Initiative Council and the SEVIN Plasma surface engineering company. A photo of an AlCrN-PVD coated compressor blade is shown in Fig. 1.

Fig. 1 - AlCrN-PVD coated compressor blade

- **Coating Qualification Tests**

Abrasion and corrosion resistance as well as hardness evaluation tests were carried out on the coated blade to ensure high quality of the coating applied. Field Emission Scanning Electron Microscopy (FE-SEM) as well as Energy Dispersive Spectroscopy (EDS) analyses were also performed to investigate the chemical composition and microstructure of the coating. It is to be noted that, the nature of the PVD technique is so as the shape, geometry and complexity of the part being coated has generally no influence on quality of the coating applied using this method. Beside this, to ensure repeatability of the process, the qualification tests were carried out on an actual blade, as well as the standard sample.

Results and Discussion

- **Coating Microstructure Examinations**

Microstructure of the AlCrN-PVD coated specimen is presented in Fig. 2. The multi-layered microstructure of the coating with an average thickness of 4 µm per layer can be seen clearly in this figure.

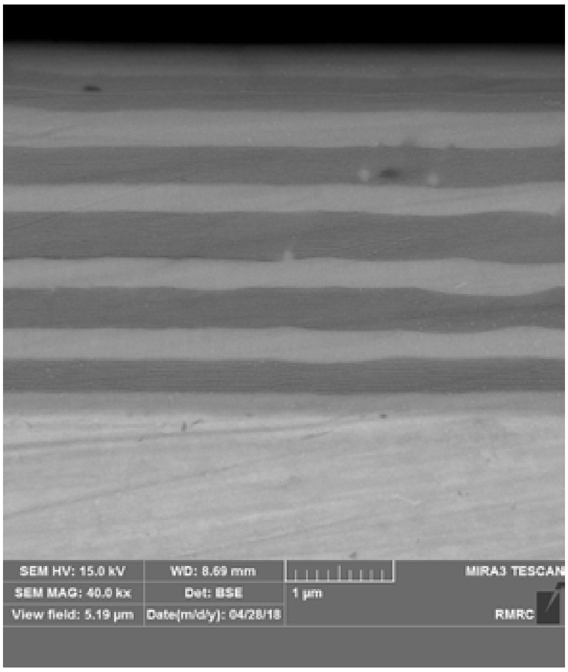

Fig. 2 - Microstructure of the AlCrN-PVD coated specimen

In order to detect the type of elements present at different layers with clear contrasts, EDS characterization was used. Fig. 3 represents the results of the EDS analysis performed on the AlCrN-PVD coated specimen with bright-white (A) and dark-gray (B) layers to be chromium and chromium-aluminum rich layers, respectively.

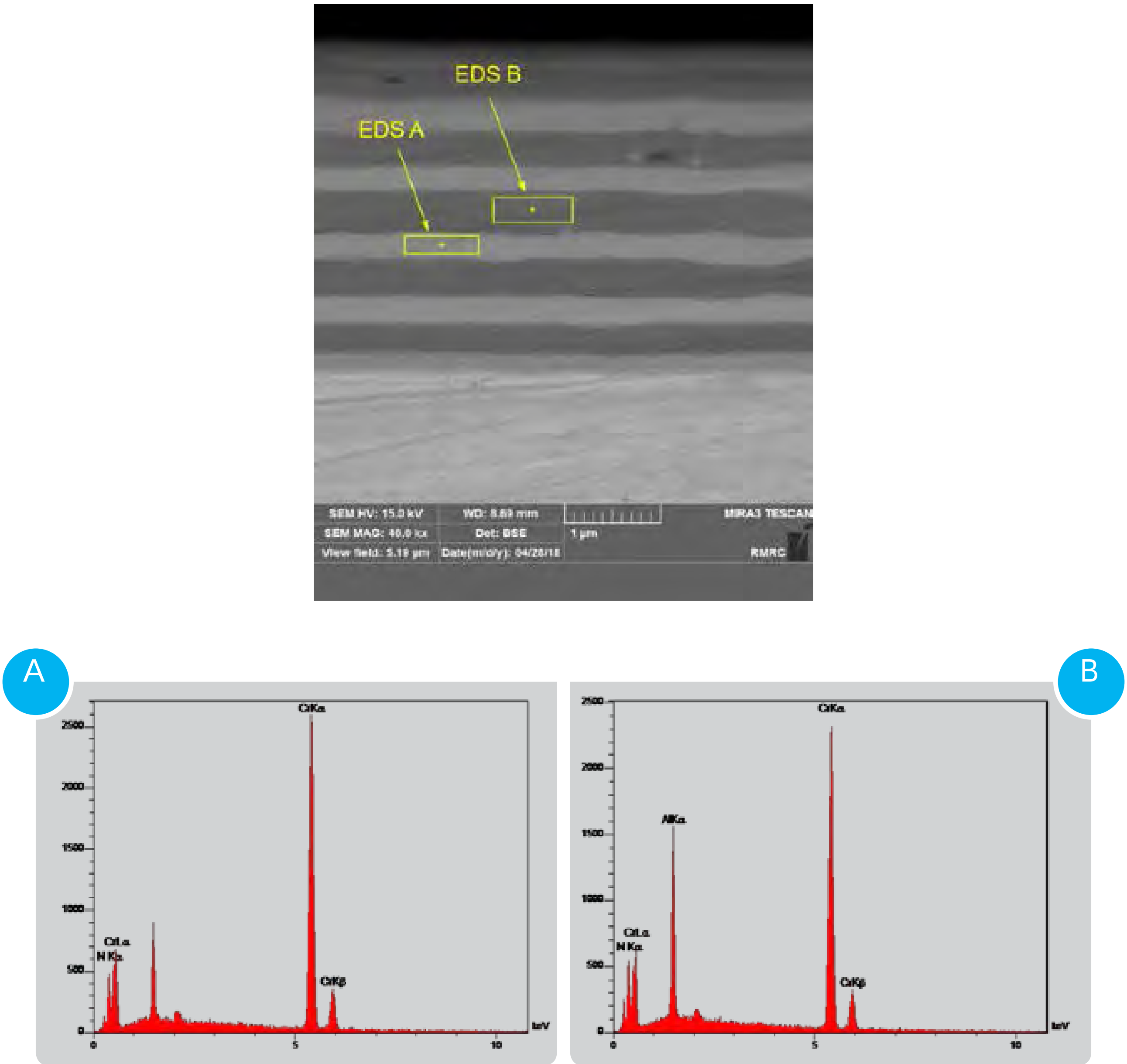

Fig 3: Results of the EDS analysis performed on the AlCrN-PVD coated specimen

Line scan analysis scattering through whole length of coating layer also demonstrated that the aluminum content of each layer increases proportionally as the chromium content decreases, as represented in Fig. 4.

As previously established in the literature, incorporation of the Aluminum into CrN leads to finer coating structures. This brings about discontinuous crystallite boundaries in the columnar structure which rules out the possibility of formation of open pores. Ding et al. [4] have also reported that alloying of binary CrN coating with aluminum to form a ternary AlCrN coating, would considerably improve the corrosion resistance of the resulting coating in aquatic solutions [4].

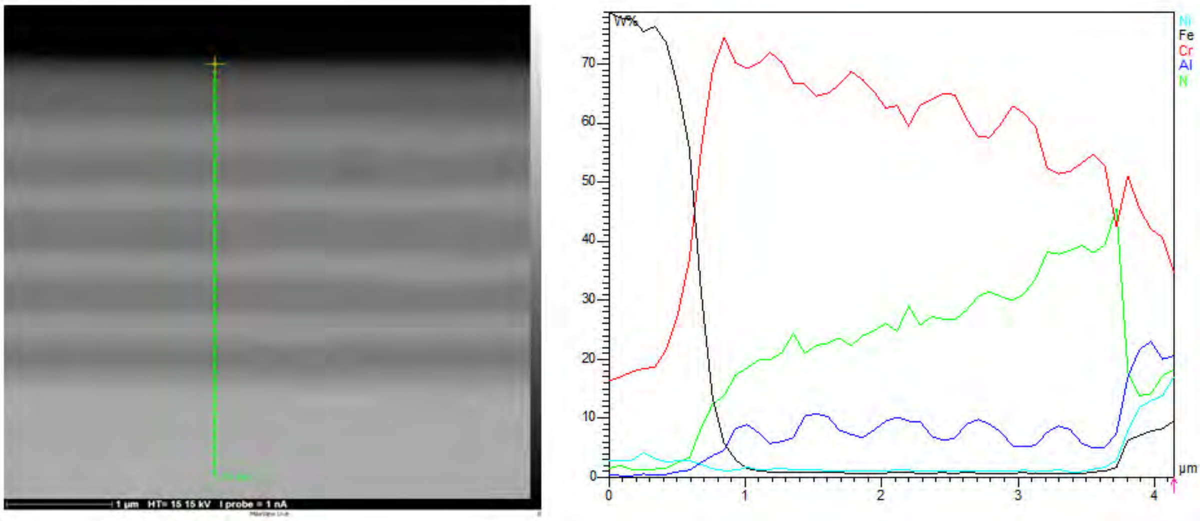

Fig 4: Results of line scan analysis performed on AlCrN-PVD coated specimen

Micro-hardness value is also considered as another indication of abrasion and erosion resistance superiority for a coating. Micro-hardness measurements were carried out on four cross-section areas of the coating layer with micro-hardness values being more than 2000 HV on average, consistent with reports that incorporation of aluminum into cubic CrN crystalline structure greatly enhances the hardness of the CrAlN coating [4].

- **Coating Macrostructure Examinations**

In addition to all micro-structural analyses performed to investigate corrosion resistance properties of the CrAlN-PVD coating applied, a standard examination test described in ASTM B 117 Standard (Salt Spray) was also carried out. Thus, coated specimens were put in a cabinet exposed to corrosive media including 3.5%wt NaCl at the temperature of 35±2 °C. The amount of time required for the first indications of corrosion i.e., red rust to be emerged, corresponds to the corrosion resistivity of the coating.

The results showed almost a 100% increase in corrosion resistance properties of the AlCrN-PVD coated specimens in comparison with the traditional i.e., aluminum pigmented ceramic coated compressor blades. It is also consistent with reports that addition of aluminum to transition metal nitrides e.g., CrN promotes corrosion resistance properties [2].

In Fig. 5 two specimens of AlCrN-PVD coated (A) and aluminum pigmented ceramic coated (B) are displayed following 200 hours of salt spray (ASTM B 117) test.

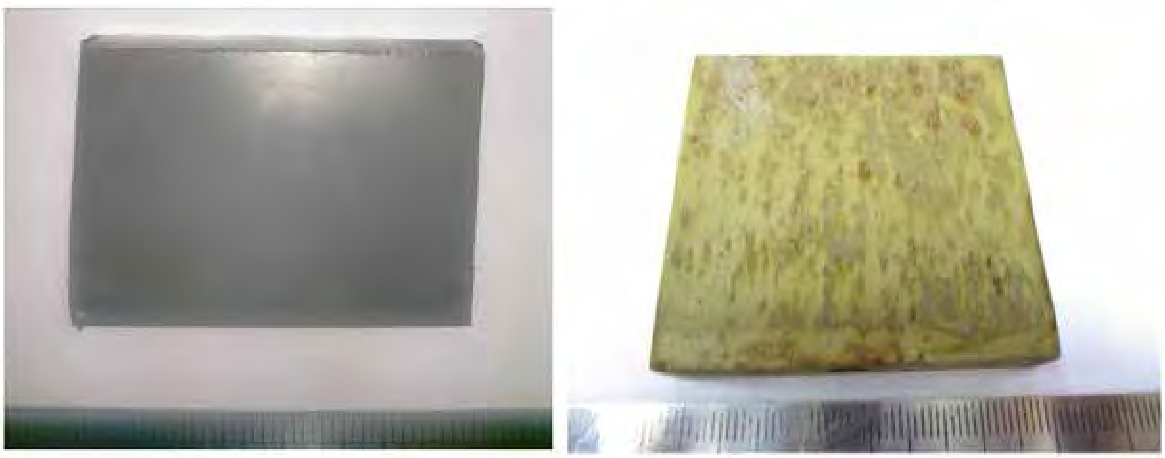

(A) (B)

Fig 5: Surface condition of AlCrN-PVD coated (A) and aluminum pigmented ceramic coated (B) specimens

An experiment based on ASTM C 1624 was also performed to evaluate abrasion resistivity of coatings. In carrying out this test, constant load method was implemented and the minimum value of the vertical force applied to reach a pre-determined failure mode was measured.

The abrasion resistance test results are presented for DLC[1]-PVD and AlCrN-PVD coated specimens in Fig. 6.

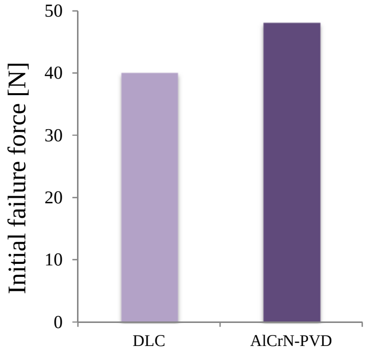

Fig 6: Scratch adhesion bar charts for the DLC and AlCrN-PVD coatings

As can be seen from this figure, the AlCrN-PVD coating shows a better performance by around 20% compared with DLC-PVD coating which is considered as a prominent hard durable film, in an abrasion resistance test setup.

Conclusions

Lowering the intake air temperature using wet compression schemes is a proven solution to improve the performance of gas turbines. In the meantime, high speed water droplets sprayed into the air intake duct or compressor section of the machine could result in an accelerated rate of abrasion and corrosion in parts such as the first stage of the compressor blades. To undermine such damage mechanisms, a special type of coating was developed and analyzed extensively through detailed micro and macro structural investigations. It was demonstrated that the AlCrN-PVD coating developed with a multi-layered microstructure, shows high abrasion resistance levels comparable and even better than those of DLC-PVD coatings and remarkably better corrosion resistance properties which makes it an effective coating to suppress abrasion and corrosion damage mechanisms in compressor blades.

The findings of the present study add more knowledge and expertise into the wide technical repertoire of MAPNA Turbine in the development and application of special protective coatings for different parts and components regardless of the application and corrosive medium involved.

References

1. B.E. Lee, K.J. Riu, S.H. Shin, S.B. Kwon, ‘Development of a water droplet erosion model for large steam turbine blades’, ASME International Journal, 17, 2003, PP.114–121.

2. V. Chawla, A. Chawla, B.S. Sidhu, S. Prakash, D. Puri, ‘Oxidation behavior of nanostructured TiAlN and AlCrN thin coatings on ASTM-SA213-T-22 boiler’, Journal of Minerals & Materials Characterization & Engineering, 9, 2010, PP.1037-1057.

3. A. Vladescu, C.M. Cotrut, A. Kiss, M. Balaceanu, V. Braic, S. Zamfir, M. Braic, ‘Corrosion resistance of the TiN, TiAlN and TiN/TiAlN nanostructured hard coatings’, UPB Science Bulletine, 68, 2006, PP. 57-64.

4. X.Z. Ding, A.L.K. Tan, X.T. Zeng, C. Wang, T. Yue, C.Q. Sun, ‘Corrosion resistance of CrAlN and TiAlN coatings deposited by lateral rotating cathode arc’, Thin Solid Films, 516, 2008, PP.5716-5720.

[1]Diamond-Like Carbon Coating

5

Experimental Investigation of Flame chemiluminescence Emission

Introduction

Flames, even in the simplest mixture and flow condition, radiate a unique spectrum of light. So, many studies have been carried out on flame spectroscopy to prove that flame emission can be used as a fingerprint to identify flame parameters. In other words, any change in flame parameters such as equivalence ratio, fuel mixture and pressure would consequently change the relevant flame emission.

Recently, optical methods have been widely used for combustion diagnostic purposes to measure important parameters such as temperature, velocity and species concentration, as these methods are non-intrusive, have suitable response time as well as high spatial resolution depending on the optical equipment used.

Among all, one of the most important fields in the combustion diagnostics is species concentration measurement. The primary standard techniques developed for this purpose such as Raman scattering and Laser-induced Fluorescence (LIF) are advanced laser-based methods. Unfortunately, implementation of these optical techniques is very complex regarding the required advanced, expensive equipment such as laser source and high speed camera.

Additionally, the chemiluminescence optical method has been considered for qualitative and semi-quantitative studies of combustion species concentration. The chemiluminescence concept is based on the light intensity measurement of the intermediate radicals resulting from combustion process and the intensity of each chemiluminescence radical is proportional to its concentration. The main advantage of this non-intrusive method is that it is simple and inexpensive in comparison with laser-based techniques.

According to the literature, it has been proved that the most important chemiluminescence radicals in hydrocarbon flames are OH*, CH* and C2*. The chemiluminescence radiation intensity of these radicals and their ratios can provide important information on the rate of chemical reactions, heat release rate, equivalence ratio, flame front location and degree of mixing. Therefore, flame chemiluminescence is considered as one of the most useful, simple and efficient techniques for practical applications in the field of combustion.

Furthermore, fluctuations of combustion systems and corresponding frequencies may be detected using this method.

Generally, flame oscillation indicates oscillation in other combustion parameters and measuring the frequency of oscillations is important for understanding dynamics of combustion systems and their monitoring.

Considering the above-mentioned potentials of chemiluminescence technique in the field of combustion and with the aim of utilization of this method in gas turbine combustor experiments, development of this technique was planned and primarily a basic chemiluminescence setup was implemented on a simple premixed burner at MAPNA Turbine combustion lab. In this R&D project, relationships between physical parameters of the flame and chemiluminescence signals were surveyed and intrinsic dynamics of the burner were also investigated.

Experimental Setup

A schematic diagram of the lab burner setup including control and measurement instruments, is presented in Fig. 1.

The experimental setup consists of two lines for supplying air and fuel, each of them equipped with required instruments to regulate burner inlet flow parameters. A simple lab burner was used to create a premixed flame conceptually similar to an advanced gas turbine burner. Natural gas was used as the fuel in the developed burner setup.

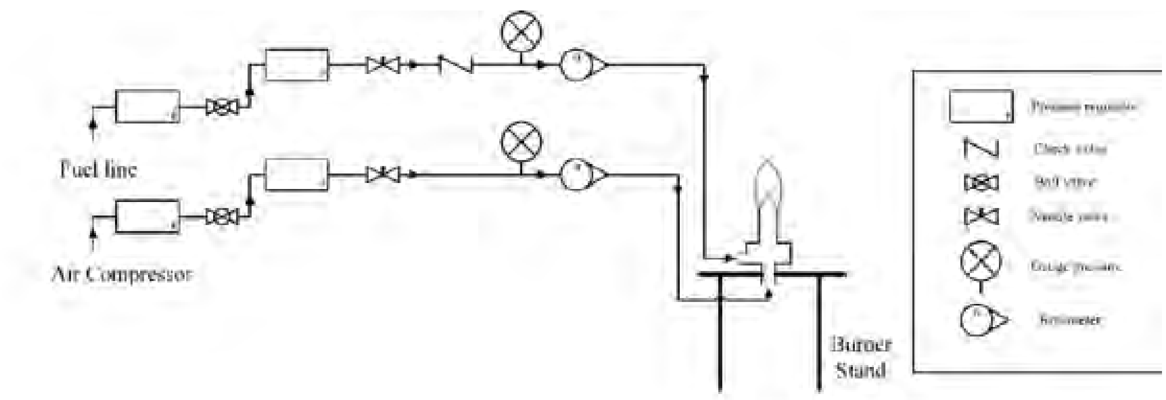

Fig. 1 – Schematic representation of the experimental burner setup

Generally, a chemiluminescence measurement setup consists of three modules of light collection and transmission, signal detection, and data processing system as shown in Fig. 2. The design of the setup and selection of the components was achieved, considering high transmission efficiency and signal to noise ratio as the fundamental criteria. Fiber optic cable with required specification is used to collect all lights emitted from the flame and transmit it to measurement module. The fiber optic head distance from the flame is also determined by acceptance angle and the maximum length of the flame, so that the entire flame fits in the fiber optic field of view.

Within the signal detection module, the light would be split into two parts using dichroic mirror to simultaneously detect CH* and OH* signals. Each part is then directed to the specific interference filter associated with chemiluminescence radicals. The selected filters have central wavelengths of 310 and 430 nm, corresponding to the CH* and OH* emissions, respectively.

Generally, CH* and OH* emission intensity is very low and cannot be detected using typical commercial sensors. Consequently, two high-tech, largely sensitive Photomultiplier Tube (PMT) sensors were used to detect these signals. The PMT output temporal electrical signal is then digitized using a 16-bit A/D card with sampling frequency of 20 kHz. In order to minimize the effects of environmental light on the measurement, all tests were done in dark and the average background signal was subtracted.

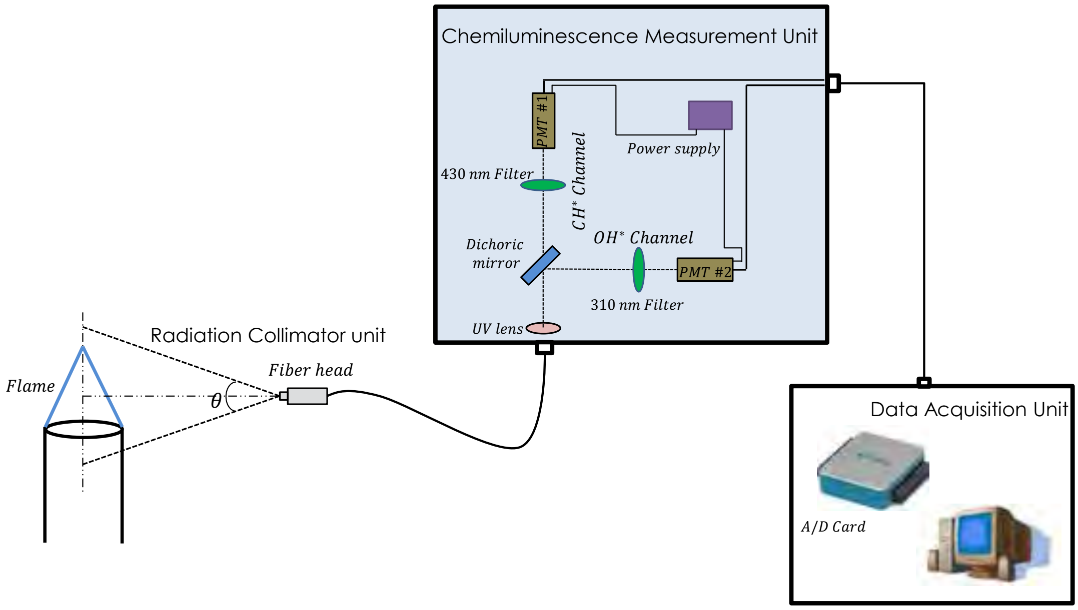

Fig. 2 – Schematic of the setup and instrumentation used for flame chemiluminescence measurements

Results & Discussion

To evaluate the performance of the designed chemiluminescence setup, a series of tests was planned and implemented. The tests covered different flame conditions including variable mixture mass flow and equivalence ratio.

The results of normalized CH* chemiluminescence signal for different equivalence ratios are shown in Fig. 3. As it is evident in this figure, by increasing the equivalence ratio from 0.88 to 1.02, the combustion approaches to the stoichiometric condition, and as a result, the CH* intensity increases. Afterwards, and up to φ = 1.4, the CH* signal decreases because of lower combustion intensity, as expected. Fig. 4 shows CH* and OH* signal variations with mixture mass flow rate for two different equivalence ratios. In both cases, CH* and OH* signals increase linearly at higher mixture mass flow rates as the reaction and heat release rates are also higher.

So, the CH* and OH* signals are deemed to be very suitable and sensitive indicators for flame reaction rate and consequently, chemiluminescence concept is used extensively in qualitative and quantitative studies to find optimal conditions in combustion systems.

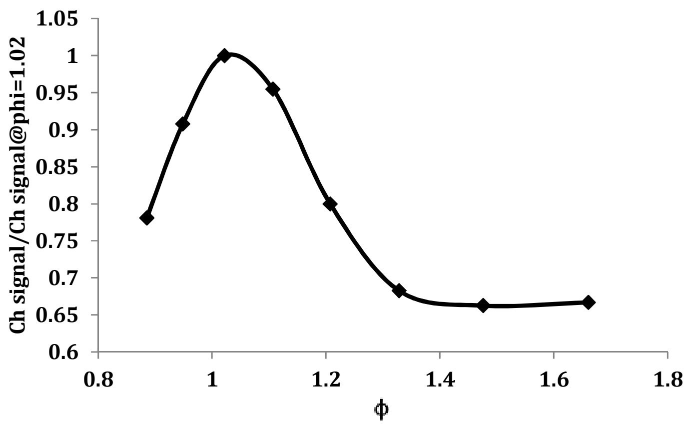

Fig. 3 – CH* signal versus equivalence ratio at m_f=10 mg/s

Fig. 5(a) shows the variation of the OH*/CH* signal in terms of mass flow rate at φ = 1.2. The difference between maximum and minimum of OH*/CH* signal in this case is about 1%. Therefore, this ratio is almost independent of the mass flow rate and depends only on the optical setup, fuel type, and equivalence ratio. Fig. 5 (b) also depicts the OH*/CH* signal versus equivalence ratio, which is commonly known as the ‘calibration graph’. Accordingly, for the present setup and in the region of φ <1.1, the OH*/CH* signal is very sensitive to the variation of the equivalence ratio, but generally for rich mixture conditions, this technique does not show enough sensitivity.

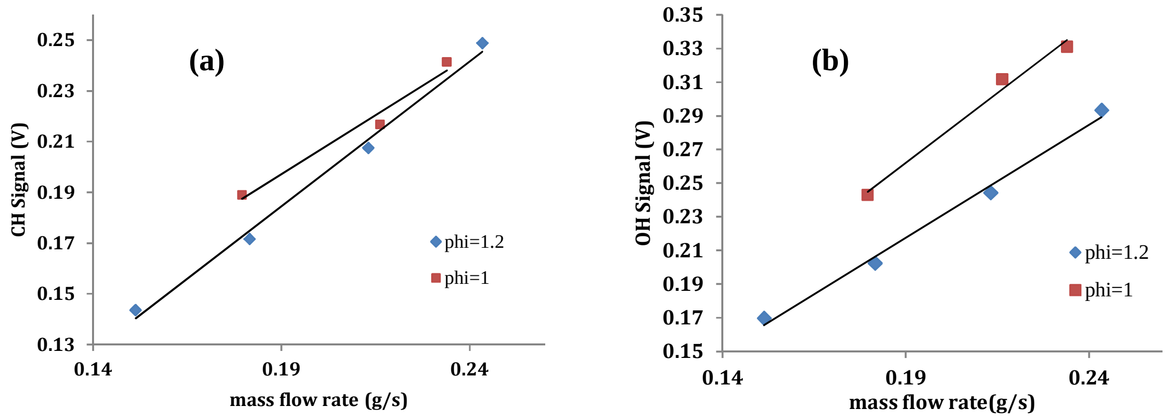

Fig. 4 – CH* (a) and OH* (b) signals versus mass flow rate

Therefore, one of the main applications of this method is control and monitoring of the equivalence ratio especially in premixed combustion systems such as DLE gas turbine combustors. The calibration graph is also applicable for local equivalence ratio monitoring, which requires development of an optical system to obtain local light from the flame [1,2].

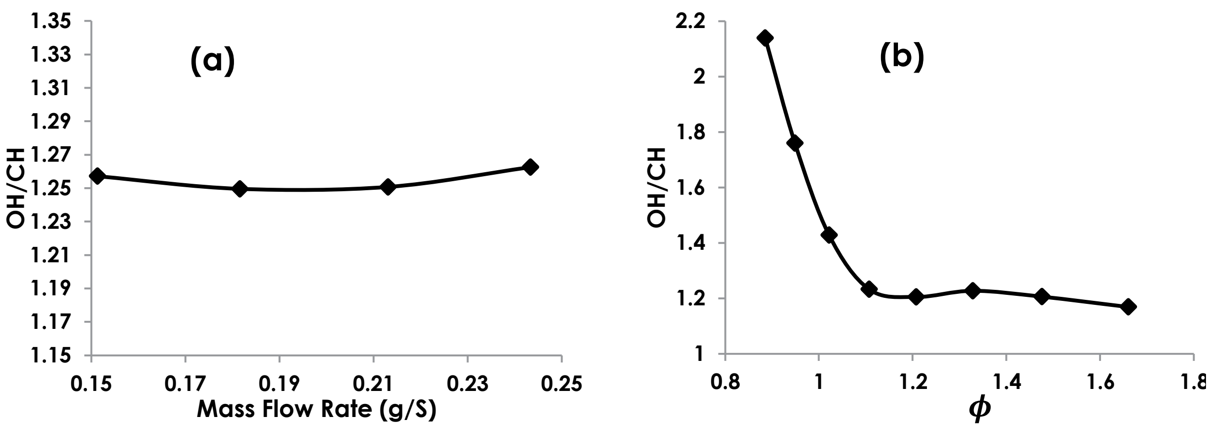

Fig. 5 – OH*/CH* versus mass flow rate at φ=1.2 (a) and OH*/CH* versus equivalence ratio (φ) at **m_f=10 mg**/s (b)

The dynamic behavior of the premixed flame was also studied in this project. As mentioned before, the CH* and OH* signals are combustion indicators. Thus, any fluctuation in the flame can be detected by these signals. Fig. 6 represents the CH*, OH* and unfiltered signals of the premixed flame in the frequency domain. For all three signals the same behavior can be observed, with the same dominant peak frequency regarding flame fluctuations. The origin of this phenomenon is usually Kelvin-Helmholtz vortices in laminar flames commonly known as ‘flame flicker’ [3, 4].

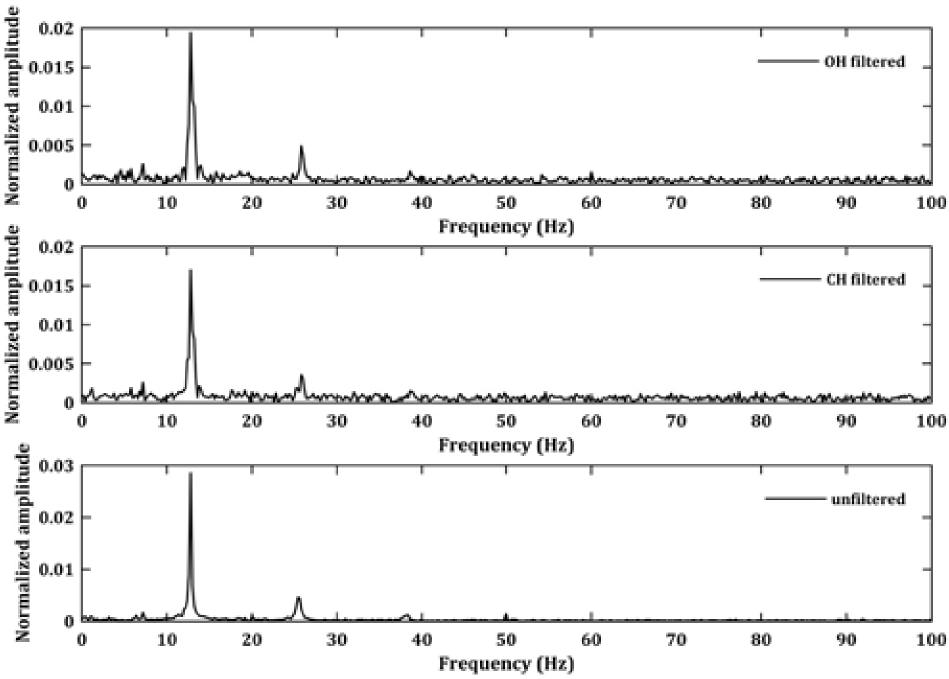

Fig. 6 – OH* (top panel), CH* (middle panel) and unfiltered (bottom panel) versus frequency signals at φ=1.66 and m_f=10 mg/s

Concluding Remarks

In this project, the chemiluminescence technique was used as one of the well-known and highly applied optical methods in the field of combustion diagnostics. Using this method, chemiluminescence emission from a premixed lab burner was identified and the OH* and CH* chemiluminescence signals were measured by PMT detectors. Also, the effects of mass flow rate and equivalence ratio on this emission were investigated. According to the results, both OH* and CH* signals are appropriate indicators of released heat rate. It was also shown that generally, OH*/CH* is independent of the mass flow rate and only affected by the equivalence ratio. Applicability of this method in characterizing combustion dynamics was also evaluated.

References

1. Y. Hardalupas, M. Orain, 'Local measurements of the time-dependent heat release rate and equivalence ratio using chemiluminescent emission from a flame', Combustion and Flame, 139(3) (2004) 188-207.
2. J. Kojima, Y. Ikeda, T. Nakajima, 'Basic aspects of OH (A), CH (A), and C2 (d) chemiluminescence in the reaction zone of laminar methane–air premixed flames', Combustion and flame, 140(1-2) (2005) 34-45.
3. D. Durox, T. Yuan, E. Villermaux, 'The effect of buoyancy on flickering in diffusion flames', Combustion science and technology, 124(1-6) (1997) 277-294.
4. I. Shepherd, R. Cheng, M. Day, 'The dynamics of flame flicker in conical premixed flames: an experimental and numerical study', Lawrence Berkeley National Laboratory, (2005).

Head Office:
231 Mirdamad Ave. Tehran, I.R.Iran.
P.O.Box: 15875-5643
Tel: +98 (21) 22908581
Fax: +98 (21) 22908654

Factory:
Mapna blvd., Fardis, Karaj, I.R.Iran.
Post code: 31676-43594
Tel: +98 (26) 36630010
Fax: +98 (26) 36612734

www.mapnaturbine.com
tr@mapnaturbine.com

GR366-0